

Deep Generalized Schrödinger Bridge

Guan-Horng Liu¹, Tianrong Chen^{1*}, Oswin So^{2*}, Evangelos A. Theodorou¹

¹Georgia Institute of Technology, USA

²Massachusetts Institute of Technology, USA

{ghliu, tianrong.chen, evangelos.theodorou}@gatech.edu
oswinso@mit.edu

Abstract

Mean-Field Game (MFG) serves as a crucial mathematical framework in modeling the collective behavior of individual agents interacting stochastically with a large population. In this work, we aim at solving a challenging class of MFGs in which the differentiability of these interacting preferences may *not* be available to the solver, and the population is urged to *converge exactly* to some desired distribution. These setups are, despite being well-motivated for practical purposes, complicated enough to paralyze most (deep) numerical solvers. Nevertheless, we show that Schrödinger Bridge — as an entropy-regularized optimal transport model — can be generalized to accepting mean-field structures, hence solving these MFGs. This is achieved via the application of Forward-Backward Stochastic Differential Equations theory, which, intriguingly, leads to a computational framework with a similar structure to Temporal Difference learning. As such, it opens up novel algorithmic connections to Deep Reinforcement Learning that we leverage to facilitate practical training. We show that our proposed objective function provides necessary and sufficient conditions to the mean-field problem. Our method, named Deep Generalized Schrödinger Bridge (**DeepGSB**), not only outperforms prior methods in solving classical population navigation MFGs, but is also capable of solving 1000-dimensional *opinion depolarization*, setting a new state-of-the-art numerical solver for high-dimensional MFGs. Our code will be made available at <https://github.com/ghliu/DeepGSB>.

1 Introduction

On a scorching morning, you navigated through the crowds toward the office. As you walked through a crosswalk, you were pondering the growing public opinion on a new policy over the past week, and were suddenly interrupted by the honking as the traffic started moving...

From navigation in crowds to propagation of opinions and traffic movement, examples of *individual agents interacting with a large population* are widespread in daily life and, due to their prevalence, appear as an important subject in multidisciplinary scientific areas, including economics [1, 2], opinion modeling [3–5], robotics [6, 7], and more recently machine learning [8–10].

Mathematically, the decision-making processes under these scenarios can be characterized by the **Mean-Field Game** [11–13] (MFG), which models a noncooperative differential game on a finite horizon between a continuum population of rational agents. Let $u(x, t)$ be the *value*

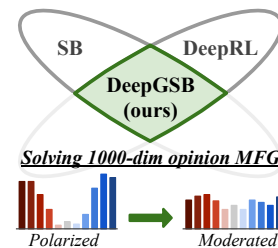


Figure 1: **DeepGSB** paves a new algorithmic connection between Schrödinger Bridge (SB) and model-based DeepRL for solving high-dimensional MFGs.

*These authors contributed equally. Work was done while Oswin was at Georgia Tech.

Table 1: Comparison to existing methods w.r.t. various desired features in Mean-Field Games (MFGs). Our **DeepGSB** is capable of solving a much wider class of MFGs in higher dimensional state spaces.

	continuous state space	stochastic MF dyn. (2)	converges to exact ρ_{target}	discontinuous MF interaction F	highest dimension
Ruthotto et al. [14]	✓	✗	✗	✗	100
Lin et al. [15]	✓	✗	✗	✗	100
Chen [16]	✗	✓	✓	✗ ¹	2
DeepGSB (ours)	✓	✓	✓	✓	1000

function, also known as optimal cost-to-goal, that governs agents’ policies at each state $x \in \mathbb{R}^d$ and time $t \in [0, T]$, and denote the resulting population density by $\rho(\cdot, t) \in \mathcal{P}(\mathbb{R}^d)$, where $\mathcal{P}(\mathbb{R}^d)$ is the set of probability measures on \mathbb{R}^d . At the Nash equilibrium where no agent has the incentive to change his/her decision, MFG, at its most general form, solves the following partial differential equations (PDEs):

$$\begin{cases} -\frac{\partial u(x,t)}{\partial t} + H(x, \nabla u, \rho) - \frac{1}{2}\sigma^2 \Delta u = F(x, \rho), & u(x, T) = G(x, \rho(\cdot, T)) \\ \frac{\partial \rho(x,t)}{\partial t} - \nabla \cdot (\rho \nabla_p H(x, \nabla u, \rho) - \frac{1}{2}\sigma^2 \Delta \rho) = 0, & \rho(x, 0) = \rho_0(x) \end{cases}, \quad (1)$$

where ∇ , $\nabla \cdot$, and Δ are respectively the gradient, divergence, and Laplacian operators.² These two PDEs are respectively known as the Hamilton-Jacobi-Bellman (HJB) and Fokker-Plank (FP) equations, which characterize the evolution of $u(x, t)$ and $\rho(x, t)$. They are coupled with each other through the Hamiltonian $H(x, p, \rho) : \mathbb{R}^d \times \mathbb{R}^d \times \mathcal{P}(\mathbb{R}^d) \rightarrow \mathbb{R}$, which describes the dynamics of the game, and the mean-field interaction $F(x, \rho) : \mathbb{R}^d \times \mathcal{P}(\mathbb{R}^d) \rightarrow \mathbb{R}$, which quantifies the agent’s preference when interacting with the population. The terminal condition G typically penalizes deviations from some desired target distribution ρ_{target} , e.g., $G \approx D_{\text{KL}}(\rho(\cdot, T) || \rho_{\text{target}}(\cdot))$. Given a solution (u, ρ) to (1), each agent acts accordingly and follows a stochastic differential equation(SDE)

$$dX_t = -\nabla_p H(X_t, \nabla u(X_t, t), \rho(\cdot, t))dt + \sigma dW_t, \quad X_0 \sim \rho_0, \quad (2)$$

where $W_t \in \mathbb{R}^d$ is the Wiener process and $\sigma \in \mathbb{R}$ is some diffusion scalar. At the mean-field limit, i.e., when the number of agents goes to infinity, the collective behavior of (2) yields the density $\rho(\cdot, t)$.

Numerical methods for solving (1) have advanced rapidly with the aid of machine learning. Seminar works such as Ruthotto et al. [14] and Lin et al. [15] approximated (u, ρ) with deep neural networks (DNNs) and directly penalized the violation of PDEs. Despite showing preliminary successes, the underlying dynamics (2) were either degenerate (e.g., $\sigma := 0$) [14], or completely discarded by instead regressing network outputs on the entire state space [15], which can scale unfavorably as the dimension d grows. An alternative that avoids both limitations, i.e., it keeps the full stochastic dynamics in (2) while being computationally scalable, is to recast these PDEs to a set of forward-backward SDEs (FBSDEs) by applying the nonlinear Feynman-Kac Lemma [17–19]. The FBSDEs analysis appears extensively in the theoretical study of MFG [20–23], yet development of scalable FBSDEs-based solver has remained, surprisingly, limited. Our work contributes to this direction.

Since ρ_{target} is known in prior, in many cases there are direct interests to seek an optimal policy that guides the agents from an initial distribution ρ_0 to the *exact* ρ_{target} , while respecting the structure of MFG, particularly the MF interaction $F(x, \rho)$. Lifting (1) to this setup, however, is highly nontrivial. Indeed, replacing the *soft* penalty at $u(x, T) = D_{\text{KL}}(\rho || \rho_{\text{target}})$ with a *hard* distributional constraint at $\rho(x, T) = \rho_{\text{target}}$ yields an HJB whose boundary condition can only be defined implicitly through FP, which now contains two distributional constraints and resembles an optimal transport problem. As such, despite being well-motivated, most prior methods have struggled to extend to this setup.

In this work, we show that **Schrödinger Bridge (SB)**, as an entropy-regularized optimal transport problem [24–28], provides an elegant recipe for solving this challenging class of *MFGs with distributional boundary constraints* $(\rho_0, \rho_{\text{target}})$. Although SB is traditionally set up with $F := 0$ [29–31], we show that SB-FBSDE [27], an FBSDE-based method for solving SB, can be generalized to accept nontrivial F ; hence solving MFG. Interestingly, the new FBSDEs system admits a similar computational structure to temporal difference (TD) learning, leading to a framework that narrows the gap

¹Precisely, Chen [16] considered discontinuous yet non-MF interaction, $F := F(x)$, on a *discrete* state space.

²These operators are taken w.r.t. x unless otherwise noted. See Appendix A.1 for the notational summary.

between SB and Deep Reinforcement Learning (DeepRL); see Fig. 1. This connection enables our method to take advantage of DeepRL techniques, such as target networks, replay buffer, actor-critic, *etc.*, and, more importantly, to handle a wide class of MF interactions that need *not* be continuous *nor* differentiable. This is in contrast to most existing works, which require differentiable [14, 15] or quadratic [32] structure on F , or discretize the state space [16]. We validate our method, called **Deep Generalized Schrödinger Bridge (DeepGSB)**, on various challenging MFGs from crowd navigation to *high-dimensional opinion depolarization* (where $d = 1000$), setting a state-of-the-art record in the area of numerical MFG solvers.

In summary, we present the following contributions.

- We present a novel numerical method, rooted in Schrödinger Bridge (SB), for solving a challenging class of Mean-Field Game where the population needs to converge *exactly* to the target distribution.
- The resulting method, **DeepGSB**, generalizes prior SB results to accepting flexible mean-field interaction (*e.g.*, non-differentiable) and enjoys modern training techniques from DeepRL.
- **DeepGSB** achieves promising empirical results in navigating crowd motion and depolarizing 1000-dimensional opinion dynamics, setting a new state-of-the-art numerical MFG solver.

2 Preliminary on Schrödinger Bridge (SB)

The SB problem was originally introduced in the 1930s for quantum mechanics [29, 33] and later draws broader interests with its connection to optimal transport and control [34–37]. Given a pair of boundary distributions (ρ_0, ρ_T) , SB seeks an optimal pair of stochastic processes of the forms:

$$dX_t = [f(X_t, t) + \sigma^2 \nabla \log \Psi(X_t, t)]dt + \sigma dW_t, \quad X_0 \sim \rho_0, \quad (3a)$$

$$d\bar{X}_s = [-f(\bar{X}_s, s) + \sigma^2 \nabla \log \widehat{\Psi}(\bar{X}_s, s)]ds + \sigma dW_s, \quad \bar{X}_0 \sim \rho_T. \quad (3b)$$

While X_t is a standard stochastic process starting from ρ_0 , \bar{X}_s evolves along the “reversed” time coordinate $s := T - t$ from ρ_T . The base drift f and diffusion σ are typically known in prior and related to the Hamiltonian H . Suppose $\Psi, \widehat{\Psi} \in C^{2,1}(\mathbb{R}^d, [0, T])$ solve the following coupled PDEs,

$$\begin{cases} \frac{\partial \Psi(x, t)}{\partial t} = -\nabla \Psi^\top f - \frac{1}{2} \sigma^2 \Delta \Psi \\ \frac{\partial \widehat{\Psi}(x, t)}{\partial t} = -\nabla \cdot (\widehat{\Psi} f) + \frac{1}{2} \sigma^2 \Delta \widehat{\Psi} \end{cases} \quad \text{s.t.} \quad \begin{cases} \Psi(\cdot, 0) \widehat{\Psi}(\cdot, 0) = \rho_0 \\ \Psi(\cdot, T) \widehat{\Psi}(\cdot, T) = \rho_T \end{cases}, \quad (4)$$

then the theory of SB suggests that the SDEs in (3) are optimal solution to an entropy-regularized (*i.e.*, minimum control) optimization problem. Furthermore, the path-wise measure induced by (3a) along $t \in [0, T]$ is equal almost surely to the path-wise measure induced by (3b) along $s := T - t$. In other words, the two SDEs in (3) can be thought of as the “reversed” process to each other; and hence we also have $X_T \sim \rho_T$ and $\bar{X}_T \sim \rho_0$ (see Fig. 2).

Due to the coupling constraints at the boundaries, solving (4) is no easier than solving (1). Fortunately, recent advances [27, 28] have demonstrated a computationally scalable numerical method via the application of the nonlinear Feynman-Kac (FK) Lemma — a mathematical tool that recasts certain classes of PDEs into sets of forward-backward SDEs (FBSDEs) via some transformation. These *nonlinear FK transformations* are parametrized in SB-FBSDE [27] by some DNNs with θ and ϕ , *i.e.*,

$$Z_\theta(\cdot, \cdot) \approx \sigma \nabla \log \Psi(\cdot, \cdot) \quad \text{and} \quad \widehat{Z}_\phi(\cdot, \cdot) \approx \sigma \nabla \log \widehat{\Psi}(\cdot, \cdot), \quad (5)$$

and the FBSDEs resulting from (4) and (5) yield the following objectives (see Appendix A.2):

$$\mathcal{L}_{\text{IPF}}(\theta) = \int_0^T \mathbb{E} \left[\frac{1}{2} \|Z_\theta(\bar{X}_s, s)\|_2^2 + Z_\theta(\bar{X}_s, s)^\top \widehat{Z}_\phi(\bar{X}_s, s) + \nabla \cdot (\sigma Z_\theta(\bar{X}_s, s) + f) \right] ds, \quad (6a)$$

$$\mathcal{L}_{\text{IPF}}(\phi) = \int_0^T \mathbb{E} \left[\frac{1}{2} \|\widehat{Z}_\phi(X_t, t)\|_2^2 + \widehat{Z}_\phi(X_t, t)^\top Z_\theta(X_t, t) + \nabla \cdot (\sigma \widehat{Z}_\phi(X_t, t) - f) \right] dt. \quad (6b)$$

The following lemma, as a direct consequence of Vargas [38], suggests that these objectives can be interpreted as the KL divergences between the parametrized path measures.

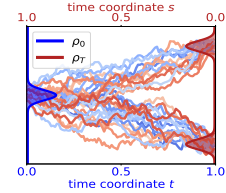


Figure 2: Simulation of the forward (3a) and backward (3b) SDEs in SB, which are minimum-energy solution when $(\Psi, \widehat{\Psi})$ obey the PDEs in (4).

Lemma 1. Let q^θ and q^ϕ be the path-wise densities of the parametrized forward and backward SDEs

$$dX_t^\theta = (f(X_t^\theta, t) + \sigma Z_\theta(X_t^\theta, t)) dt + \sigma dW_t, \quad d\bar{X}_s^\phi = \left(-f(\bar{X}_s^\phi, t) + \sigma \widehat{Z}_\phi(\bar{X}_s^\phi, t)\right) ds + \sigma dW_s.$$

Then, we have

$$D_{\text{KL}}(q^\theta || q^\phi) \propto \mathcal{L}_{\text{IPF}}(\phi), \quad \text{and} \quad D_{\text{KL}}(q^\phi || q^\theta) \propto \mathcal{L}_{\text{IPF}}(\theta).$$

Proof. See Appendix A.3.2. □

Lemma 1 suggests that alternative minimization between $\mathcal{L}_{\text{IPF}}(\phi)$ and $\mathcal{L}_{\text{IPF}}(\theta)$ is equivalent to performing iterative KL projection [39], and is hence equivalent to applying the Iterative Proportional Fitting [40] (IPF) algorithm to solve parametrized SBs [24, 25].

3 Deep Generalized Schrödinger Bridge (DeepGSB)

3.1 Connection between the coupled PDEs in MFG and SB

We begin by first stating our problem of interest — MFG with hard distributional constraints $(\rho_0, \rho_{\text{target}})$ — in its mathematical form. Similar to prior works [14, 15], we will adopt the control-affine Hamiltonian, $H(x, \nabla u, \rho) := \frac{1}{2} \|\sigma \nabla u\|^2 - \nabla u^\top f(x, \rho)$, given some base drift f and diffusion scalar σ . Substituting this control-affine Hamiltonian into the PDEs in (1) yields

$$\begin{cases} -\frac{\partial u(x,t)}{\partial t} + \frac{1}{2} \|\sigma \nabla u\|^2 - \nabla u^\top f - \frac{1}{2} \sigma^2 \Delta u = F(x, \rho), \\ \frac{\partial \rho(x,t)}{\partial t} - \nabla \cdot (\rho (\sigma^2 \nabla u - f)) - \frac{1}{2} \sigma^2 \Delta \rho = 0, \quad \rho(x, 0) = \rho_0(x), \rho(x, T) = \rho_{\text{target}}(x), \end{cases} \quad (7)$$

which, as we briefly discussed in Sec.1, differ from (1) in that the boundary condition of the HJB, $u(x, T)$, is now absorbed into FP and defined implicitly through $\rho(x, T) = \rho_{\text{target}}(x)$. Since analytic conversion between the boundary conditions of (1) and (7) exists only for highly degenerate³ cases [41], this seemingly innocuous change suffices to paralyze most prior methods.⁴ Nevertheless, as (7) now describes a transformation between two distributions (from FP) while obeying some optimality (from HJB), it suggests a deeper connection to optimal transport, and hence the SB.

To bridge these new MFG PDEs (7) to the PDEs appearing in SB (4), we follow standard treatment [30] and apply the Hopf-Cole transform [42, 43]:

$$\Psi(x, t) := \exp(-u(x, t)), \quad \widehat{\Psi}(x, t) := \rho(x, t) \exp(u(x, t)), \quad (8)$$

which, after some algebra (see Appendix A.4.1 for details), yields the following PDEs:

$$\begin{cases} \frac{\partial \Psi(x,t)}{\partial t} = -\nabla \Psi^\top f - \frac{1}{2} \sigma^2 \Delta \Psi + F \Psi \\ \frac{\partial \widehat{\Psi}(x,t)}{\partial t} = -\nabla \cdot (\widehat{\Psi} f) + \frac{1}{2} \sigma^2 \Delta \widehat{\Psi} - F \widehat{\Psi} \end{cases} \quad \text{s.t.} \quad \begin{cases} \Psi(\cdot, 0) \widehat{\Psi}(\cdot, 0) = \rho_0 \\ \Psi(\cdot, T) \widehat{\Psi}(\cdot, T) = \rho_{\text{target}} \end{cases}. \quad (9)$$

It can be seen that (9) generalizes (4) by introducing the MF interaction F . Let $(\Psi, \widehat{\Psi})$ be the solution to these new MF-extended PDEs in (9), and recall the Hamiltonian adopted in (7), one can find that

$$-\nabla_p H(X_t, \nabla u, \rho) = f - \sigma^2 \nabla u = f + \sigma^2 \nabla \log \Psi.$$

That is, the agent's dynamic (2) coincides with the forward SDE (3a) in SB. Hence, we have connected the MFG (1) and SB (4) frameworks through the PDEs in (7) and (9); see Fig. 3.

³Zhang and Chen [41] suggested $F := 0$, $f := f(x)$ and ρ_0 a degenerate Dirac delta distribution.

⁴For completeness, we note that when the base drift is independent of the density, $f := f(x)$, and mean-field preference, $\mathcal{F}(\rho) : F(x, \rho) = \frac{\delta \mathcal{F}}{\delta \rho}$, is convex in ρ , the variational optimization inherited in (7) remains convex. In these cases, the discretized problems converge to the global solution [16, 32]. However, for generic mean-field dynamics, such as the polarized $f(x, \rho)$ in our (18), the problem is in general non-convex; hence only local convergence can be established (see e.g., Remark 1 in [16]).

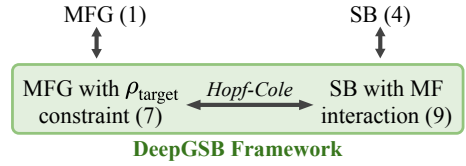


Figure 3: Connection between different coupled PDEs appearing in MFG, SB, and DeepGSB.

3.2 Generalized SB-FBSDEs with mean-field interaction

With (9), we are ready to present our result that generalizes prior FBSDE for SB to MF interaction.

Theorem 2 (Generalized SB-FBSDEs). *Suppose $\Psi, \widehat{\Psi} \in C^{2,1}$ and let f, F satisfy usual growth and Lipschitz conditions [44, 45]. Consider the following nonlinear FK transformations applied to (9):*

$$\begin{aligned} Y_t &\equiv Y(X_t, t) = \log \Psi(X_t, t), & Z_t &\equiv Z(X_t, t) = \sigma \nabla \log \Psi(X_t, t), \\ \widehat{Y}_t &\equiv \widehat{Y}(X_t, t) = \log \widehat{\Psi}(X_t, t), & \widehat{Z}_t &\equiv \widehat{Z}(X_t, t) = \sigma \nabla \log \widehat{\Psi}(X_t, t), \end{aligned} \quad (10)$$

where X_t follows (3a) with $X_0 \sim \rho_0$. Then, the resulting FBSDEs system takes the form:

$$\begin{aligned} \text{FBSDEs} &: \begin{cases} dX_t = (f_t + \sigma Z_t) dt + \sigma dW_t & (11a) \\ dY_t = \left(\frac{1}{2} \|Z_t\|^2 + F_t \right) dt + Z_t^\top dW_t & (11b) \\ d\widehat{Y}_t = \left(\frac{1}{2} \|\widehat{Z}_t\|^2 + \nabla \cdot (\sigma \widehat{Z}_t - f_t) + \widehat{Z}_t^\top Z_t - F_t \right) dt + \widehat{Z}_t^\top dW_t & (11c) \end{cases} \\ \text{w.r.t. (3a)} & \end{aligned}$$

Now, consider a similar transformation in (9) but instead w.r.t. the ‘‘reversed’’ SDE $\bar{X}_s \sim (3b)$ and $\bar{X}_0 \sim \rho_{\text{target}}$, i.e., $Y_s \equiv Y(\bar{X}_s, s) = \log \Psi(\bar{X}_s, s)$, and etc. The resulting FBSDEs system reads

$$\begin{aligned} \text{FBSDEs} &: \begin{cases} d\bar{X}_s = (-f_s + \sigma \widehat{Z}_s) ds + \sigma dW_s & (12a) \\ dY_s = \left(\frac{1}{2} \|Z_s\|^2 + \nabla \cdot (\sigma Z_s + f_s) + Z_s^\top \widehat{Z}_s - F_s \right) ds + Z_s^\top dW_s & (12b) \\ d\widehat{Y}_s = \left(\frac{1}{2} \|\widehat{Z}_s\|^2 + F_s \right) ds + \widehat{Z}_s^\top dW_s & (12c) \end{cases} \\ \text{w.r.t. (3b)} & \end{aligned}$$

Since $Y_t + \widehat{Y}_t = \log \rho(X, t)$ by construction, the functions f_t and F_t in (11) take the arguments

$$f_t := f_t(X_t, \exp(Y_t + \widehat{Y}_t)) \quad \text{and} \quad F_t := F_t(X_t, \exp(Y_t + \widehat{Y}_t)).$$

Similarly, we have $f_s := f_s(\bar{X}_s, \exp(Y_s + \widehat{Y}_s))$ and $F_s := F_s(\bar{X}_s, \exp(Y_s + \widehat{Y}_s))$ in (12).

Proof. See Appendix A.3.3. □

Just like how (9) generalizes (4), our results in Theorem 2 also generalize the ones appearing in vanilla SB-FBSDE [27] (see (22) in Appendix A.2) by introducing nontrivial MF interaction F . Despite seemingly complex compared to the original PDEs (9), these FBSDEs systems — namely (11) and (12) — stand as the foundation for developing scalable numerical methods, as they describe precisely how the values of $Y \equiv \log \Psi$ and $\widehat{Y} \equiv \log \widehat{\Psi}$ shall change along the optimal SDEs (notice, e.g., that both Y_t and Z_t are functions of X_t from (10)). Essentially, the nonlinear FK Lemma provides a stochastic representation (in terms of Y and \widehat{Y}) of the PDEs in (9) by expanding them w.r.t. the optimal SDEs in (3) using the Itô formula [46]. Consequently, rather than solving the PDEs (9) in the *entire function space* as in the prior work [15], it suffices to solve them *locally around high probability regions* characterized by (3), which leads to computationally scalable methods.

3.3 Design of the computational framework

Looking from Theorem 2, it suffices to approximate $Y_\theta \approx Y$ and $\widehat{Y}_\phi \approx \widehat{Y}$ with some parametrized functions (we use DNNs), since one may infer $Z_\theta \approx \sigma \nabla Y_\theta$ and $\widehat{Z}_\phi \approx \sigma \nabla \widehat{Y}_\phi$, as suggested by (10), and then solve for (X_t, \bar{X}_s) via (11a, 12a). Below, we explore options of designing training objectives for (θ, ϕ) , with the aim to encourage $(Y_\theta, \widehat{Y}_\phi)$ to satisfy the FBSDEs systems in (11, 12).

Option 1: \mathcal{L}_{IPF} . Given how Theorem 2 generalizes the one in [27] (see (22) in Appendix A.2), it is natural to wonder if adopting the computation used to derive (6), e.g., $\mathcal{L}_{\text{IPF}}(\phi) := \int \mathbb{E}[dY_t^\theta + d\widehat{Y}_t^\phi]$,⁵

⁵Additionally, we have $\mathcal{L}_{\text{IPF}}(\theta) := \int \mathbb{E}[dY_s^\theta + d\widehat{Y}_s^\phi]$; see (24) in Appendix A.2 for the derivation.

suffices to reach the FBSDE (11). This is, unfortunately, not the case as one can verify that

$$\mathcal{L}_{\text{IPF}}^{(11)}(\phi) := \int \mathbb{E} \left[dY_t^\theta + d\widehat{Y}_t^\phi \right] = \int \mathbb{E} \left[\frac{1}{2} \|\widehat{Z}_t^\phi + Z_t^\theta\|^2 + \nabla \cdot (\sigma \widehat{Z}_t^\phi - f) \right] dt = \mathcal{L}_{\text{IPF}}^{(6b)}(\phi).$$

Despite that (11) differs from (22) by the extra terms “ $+F_t$ ” in (11b) and “ $-F_t$ ” in (11c), the two terms cancel out in the sum of $dY_t^\theta + d\widehat{Y}_t^\phi$, thereby yielding the same objectives that *do not depend on F* . This implies that naively optimizing \mathcal{L}_{IPF} from [27] is insufficient for solving FBSDE systems with nontrivial F . We must seek additional objectives, if any, in order to respect the MF structure.

Option 2: \mathcal{L}_{IPF} + Temporal Difference objective \mathcal{L}_{TD} . Let us revisit the relation between the FBSDEs (11, 12) and their PDEs counterparts — but this time the HJB in (7). Take (X_t, Y_t) for example: The fact that $Y_t = \log \Psi(X_t, t) = -u(X_t, t)$ suggests an alternative interpretation of Y_t as the stochastic representation of the HJB, which, crucially, can be seen as the continuous-time analogue of the Bellman equation [47]. Indeed, discretizing (11b) with some fixed step size δt yields

$$Y_{t+\delta t}^\theta = Y_t^\theta + \left(\frac{1}{2} \|Z_t^\theta\|^2 + F_t \right) \delta t + Z_t^{\theta \top} \delta W_t, \quad \delta W_t \sim \mathcal{N}(\mathbf{0}, \delta t \mathbf{I}), \quad (13)$$

which resembles a (non-discounted) Temporal Difference (TD) [48, 49] except that, in addition to the standard “*rewards*” (in terms of control and state costs), we also have a **stochastic term**. This stochastic term, which vanishes in the vanilla Bellman equation upon taking expectations, plays a crucial role in characterizing the inherited stochasticity of the value function Y_t . With this interpretation in mind, we can construct suitable TD targets for our FBSDEs systems as shown below.

Proposition 3 (TD objectives \mathcal{L}_{TD} for (11, 12)). *The single-step TD targets take the forms:*

$$\widehat{\text{TD}}_{t+\delta t}^{\text{single}} := \widehat{Y}_t^\phi + \left(\frac{1}{2} \|\widehat{Z}_t^\phi\|^2 + \nabla \cdot (\sigma \widehat{Z}_t^\phi - f_t) + \widehat{Z}_t^{\phi \top} Z_t^\theta - F_t \right) \delta t + \widehat{Z}_t^{\phi \top} \delta W_t, \quad (14a)$$

$$\text{TD}_{s+\delta s}^{\text{single}} := Y_s^\theta + \left(\frac{1}{2} \|Z_s^\theta\|^2 + \nabla \cdot (\sigma Z_s^\theta + f_s) + Z_s^{\theta \top} \widehat{Z}_s^\phi - F_s \right) \delta s + Z_s^{\theta \top} \delta W_s, \quad (14b)$$

with $\widehat{\text{TD}}_0 := \log \rho_0 - Y_0^\theta$ and $\text{TD}_0 := \log \rho_{\text{target}} - \widehat{Y}_0^\phi$, and the multi-step TD targets take the forms:

$$\widehat{\text{TD}}_{t+\delta t}^{\text{multi}} := \widehat{\text{TD}}_0 + \sum_{\tau=\delta t}^t \delta \widehat{Y}_\tau, \quad \text{TD}_{s+\delta s}^{\text{multi}} := \text{TD}_0 + \sum_{\tau=\delta s}^s \delta Y_\tau, \quad (15)$$

where $\delta \widehat{Y}_t := \widehat{\text{TD}}_{t+\delta t}^{\text{single}} - \widehat{Y}_t$ and $\delta Y_s := \text{TD}_{s+\delta s}^{\text{single}} - Y_s$. Given these TD targets, we can construct

$$\mathcal{L}_{\text{TD}}(\theta) = \sum_{s=0}^T \mathbb{E} [\|Y_\theta(\bar{X}_s, s) - \text{TD}_s\|] \delta s, \quad \mathcal{L}_{\text{TD}}(\phi) = \sum_{t=0}^T \mathbb{E} [\|\widehat{Y}_\phi(X_t, t) - \widehat{\text{TD}}_t\|] \delta t. \quad (16)$$

Proof. See Appendix A.3.4. □

It can be readily seen that the single-step TD targets in (14) obey a similar structure to (13), except deriving from different SDEs (11c, 12b). Doing so reduces the computational overhead, as the related objectives for each parameter, *e.g.*, $\mathcal{L}_{\text{IPF}}(\theta)$ and $\mathcal{L}_{\text{TD}}(\theta)$, can be evaluated from the same expectation. In practice, we find that the multi-step objectives often yield better performance, as consistently observed in the DeepRL literature [50–52]. Additionally, common practices such as computing $\widehat{\text{TD}}_t$ and TD_s using the exponential moving averaging (*i.e.*, target values) and replay buffers also help stabilize training. Finally, the fact that the TD targets in (16) appear as the regressands implies that from a computational standpoint, the MF interaction F needs *not* to be continuous or differentiable.

Necessity and sufficiency of \mathcal{L}_{IPF} + \mathcal{L}_{TD} . It remains unclear whether appending \mathcal{L}_{TD} to the objective suffices for $(Y_\theta, \widehat{Y}_\phi)$ to satisfy the FBSDEs (11, 12). Below, we provide a positive result.

Proposition 4. *The functions $(Y_\theta, Z_\theta, \widehat{Y}_\phi, \widehat{Z}_\phi)$ satisfy the FBSDEs (11, 12) in Theorem 2 if and only if they are the minimizers of the combined losses $\mathcal{L}(\theta, \phi) := \mathcal{L}_{\text{IPF}}(\phi) + \mathcal{L}_{\text{TD}}(\phi) + \mathcal{L}_{\text{IPF}}(\theta) + \mathcal{L}_{\text{TD}}(\theta)$.*

Proof. See Appendix A.3.5. □

Algorithm 1 Deep Generalized Schrödinger Bridge (DeepGSB)

Input: $(Y_\theta, \widehat{Y}_\phi, \sigma \nabla Y_\theta, \sigma \nabla \widehat{Y}_\phi)$ for critic or $(Y_\theta, \widehat{Y}_\phi, Z_\theta, \widehat{Z}_\phi)$ for actor-critic parametrization.
repeat
 Sample $\mathbf{X}^\theta \equiv \{X_t^\theta, Z_t^\theta, \delta W_t\}_{t \in [0, T]}$ from the forward SDE (11a); add \mathbf{X}^θ to replay buffer \mathcal{B} .
 for $k = 1$ **to** K **do**
 Sample on-policy $\mathbf{X}_{\text{on}}^\theta$ and off-policy $\mathbf{X}_{\text{off}}^\theta$ samples respectively from \mathbf{X}^θ and \mathcal{B} .
 Compute $\mathcal{L}(\phi) = \mathcal{L}_{\text{IPF}}(\phi; \mathbf{X}_{\text{on}}^\theta) + \mathcal{L}_{\text{TD}}(\phi; \mathbf{X}_{\text{on}}^\theta) + \mathcal{L}_{\text{TD}}(\phi; \mathbf{X}_{\text{off}}^\theta) + \mathcal{L}_{\text{FK}}(\phi; \mathbf{X}_{\text{on}}^\theta)$.
 Update ϕ with the gradient $\nabla_\phi \mathcal{L}(\phi)$.
 end for
 Sample $\bar{\mathbf{X}}^\phi \equiv \{\bar{X}_s^\phi, \widehat{Z}_s^\phi, \delta W_s\}_{s \in [0, T]}$ from the backward SDE (12a); add $\bar{\mathbf{X}}^\phi$ to replay buffer $\bar{\mathcal{B}}$.
 for $k = 1$ **to** K **do**
 Sample on-policy $\bar{\mathbf{X}}_{\text{on}}^\phi$ and off-policy $\bar{\mathbf{X}}_{\text{off}}^\phi$ samples respectively from $\bar{\mathbf{X}}^\phi$ and $\bar{\mathcal{B}}$.
 Compute $\mathcal{L}(\theta) = \mathcal{L}_{\text{IPF}}(\theta; \bar{\mathbf{X}}_{\text{on}}^\phi) + \mathcal{L}_{\text{TD}}(\theta; \bar{\mathbf{X}}_{\text{on}}^\phi) + \mathcal{L}_{\text{TD}}(\theta; \bar{\mathbf{X}}_{\text{off}}^\phi) + \mathcal{L}_{\text{FK}}(\theta; \bar{\mathbf{X}}_{\text{on}}^\phi)$.
 Update θ with the gradient $\nabla_\theta \mathcal{L}(\theta)$.
 end for
until converges

Proposition 4 asserts the validity of the combined objectives $\mathcal{L}_{\text{IPF}} + \mathcal{L}_{\text{TD}}$ in solving the generalized SB-FBSDEs in Theorem 2, and hence the MFG problem in (7). It shall be interpreted as follows: The minimizer of \mathcal{L}_{IPF} , as implied in Lemma 1, would always establish a valid “bridge” transporting between the boundary distributions ρ_0 and ρ_{target} ; yet, without further conditions, this bridge needs not obey a “Schrödinger” bridge. While general IPF and Sinkhorn [16, 32], upon proper initialization or discretization, provides one way to ensure the convergence toward the “S”B, our Proposition 4 suggests an alternative by introducing the TD objectives \mathcal{L}_{TD} . This gives us flexibility to handle generalized SB in MFGs where F becomes nontrivial or non-convex. Further, it naturally handles non-differentiable F , which can offer extra benefits in many cases.

Option 3: $\mathcal{L}_{\text{IPF}} + \mathcal{L}_{\text{TD}} + \text{FK objective } \mathcal{L}_{\text{FK}}$. Though it seems sufficient to parametrize $(Y_\theta, \widehat{Y}_\phi)$ then infer $Z_\theta := \sigma \nabla Y_\theta$ and $\widehat{Z}_\phi := \sigma \nabla \widehat{Y}_\phi$, as suggested in previous options, in practice we find that parametrizing $(Z_\theta, \widehat{Z}_\phi)$ with two additional DNNs then imposing the following FK objective, *i.e.*,

$$\mathcal{L}_{\text{FK}}(\theta) = \sum_{s=0}^T \mathbb{E} [\|\sigma \nabla Y_\theta(\bar{X}_s, s) - Z_\theta(\bar{X}_s, s)\|] \delta s, \quad \mathcal{L}_{\text{FK}}(\phi) = \sum_{t=0}^T \mathbb{E} [\|\sigma \nabla \widehat{Y}_\phi(X_t, t) - \widehat{Z}_\phi(X_t, t)\|] \delta t,$$

often offers extra robustness. These objectives aim to ensure that the nonlinear FK (10) holds.

Our **DeepGSB** is summarized in Alg. 1. Hereafter, we refer Option 2 and 3 respectively to *DeepGSB critic* and *DeepGSB actor-critic*, as Y_θ and Z_θ play similar roles of critic and actor networks [53, 54].

Remarks on convergence. Despite Alg. 1 sharing a similar alternating structure to IPF [16, 24, 27], the combined objective, *e.g.*, $\mathcal{L}(\phi) \propto D_{\text{KL}}(\rho^\theta || \rho^\phi) + \mathbb{E}_{\rho^\theta}[\mathcal{L}_{\text{TD}}(\phi)] \neq D_{\text{KL}}(\rho^\phi || \rho^\theta)$ is *not* equivalent to the (reversed) KL appearing in IPF. Instead, DeepGSB may be closer to trust region optimization [55], as both iteratively update the policy using samples from the previous stage while subjected to some KL penalty: $\pi^{(i+1)} = \arg \min_{\pi} D_{\text{KL}}(\pi^{(i)} || \pi) + \mathbb{E}_{\pi^{(i)}}[\mathcal{L}(\pi)]$. Hence, one can expect DeepGSB to admit similar monotonic improvement and local convergence properties. We leave more discussions to Appendix A.4.2.

4 Experiment

Instantiation of MFGs. We validate our DeepGSB on two classes of MFGs, including classical crowd navigation ($d=2$) and high-dimensional ($d=1000$) opinion depolarization. For crowd navigation, we consider three MFGs appearing in prior methods [14, 15], including (i) asymmetric obstacle avoidance, (ii) entropy interaction with a V-shape bottleneck, and (iii) congestion interaction on an S-shape tunnel. We will refer to them respectively as **GMM**, **V-neck**, and **S-tunnel**. The obstacles and the initial/target Gaussian distributions ($\rho_0, \rho_{\text{target}}$) are shown in Fig. 4. For opinion depolarization, we set ρ_0 and ρ_{target} to two zero-mean Gaussians with varying variances for representing the initially polarized and desired moderated opinion distributions. Finally, we consider zero and constant base drift f respectively for GMM and V-neck/S-tunnel, and adopt the polarized MF dynamics [4] for opinion MFG; see Sec. 4.2 for a detailed discussion.

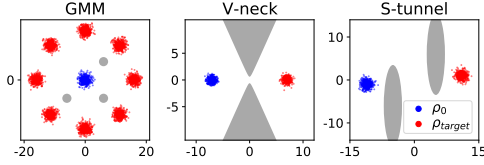


Figure 4: Crowd navigation MFGs.

Table 2: MF interactions for 3 crowd navigation MFGs and the high-dimensional opinion MFG.

GMM ($d=2$)	F_{obstacle}
V-neck ($d=2$)	$F_{\text{obstacle}} + F_{\text{entropy}}$
S-tunnel ($d=2$)	$F_{\text{obstacle}} + F_{\text{congestion}}$
Opinion ($d=1000$)	F_{entropy}

MF interactions F . We follow standard treatments from the MFG theory [11] by noting that given a functional $\mathcal{F}(\rho)$ that quantifies the MF cost w.r.t. the population ρ , *e.g.*, $\mathcal{F}_{\text{entropy}} := \mathbb{E}_{\rho}[\log \rho]$ or $\mathcal{F}_{\text{congestion}} := \mathbb{E}_{x,y \sim \rho} \left[\frac{1}{\|x-y\|^2+1} \right]$, one can derive its associated MF interaction function $F(x, \rho)$ by taking the functional derivative, *i.e.*, $\frac{\delta \mathcal{F}(\rho)}{\delta \rho}(x) = F(x, \rho)$. Hence, the entropy and congestion MF interactions, together with the obstacle cost, follow (see Appendix A.4.3 for the derivation):

$$F_{\text{entropy}} := \log \rho(x, t) + 1, \quad F_{\text{congestion}} := \mathbb{E}_{y \sim \rho} \left[\frac{2}{\|x-y\|^2+1} \right], \quad F_{\text{obstacle}} := 1500 \cdot \mathbb{1}_{\text{obs}}(x), \quad (17)$$

where $\mathbb{1}_{\text{obs}}(\cdot)$ is the (discontinuous) indicator of the problem-dependent obstacle set. We summarize the MF interaction in Table 2.

Architecture & Hyperparameters. We parameterize the functions with fully-connected DNNs for crowd navigation, and deep residual networks for high-dimensional opinion MFGs. All networks adopt sinusoidal time embeddings and are trained with AdamW [56]. All SDEs in (11, 12) are solved with the Euler-Maruyama method. Due to space constraints, we will focus mostly on the results of actor-critic parametrization **DeepGSB-ac**, and leave the discussion of critic parametrization **DeepGSB-c**, along with additional experimental details, to Appendix A.5.

4.1 Two-dimensional crowd navigation

Figure 5 shows the simulation results of our **DeepGSB-ac** on three crowd navigation MFGs. We also report existing numerical methods [14–16] that are best-tuned on each MFG (see Appendix A.5.1 for details) but note that in practice, they either require softening F to be differentiable [14, 15] to yield reasonable results, or discretizing the state space [16], which can lead to prohibitive complexity.⁶

We first compare to Chen [16] on **GMM** (see Fig. 5a) as their method only applies to non-MF interaction, *i.e.*, $F := F(x)$. While **DeepGSB-ac** guides the population to smoothly avoid all obstacles (notice the sharp contours of Y around them), [16] struggles to escape due to the discretization of the state space (hence the policy). To better examine the effect of ρ in $F(x, \rho)$, we next simulate the dynamics on **V-neck** (see Fig. 5b) with and without the MF interaction. It is clear that our **DeepGSB-ac** encourages the population to spread out once the entropy interaction F_{entropy} is enabled, yet a similar effect is barely observed in [14]. We observed difficulties in balancing the MF interaction F and the terminal penalty $D_{\text{KL}}(\rho_T \parallel \rho_{\text{target}})$ for [14], yet this problem is alleviated in DeepGSB by construction. Lastly, we validate the robustness of our method on **S-tunnel** (see Fig. 5c) w.r.t. varying diffusions $\sigma = \{0.5, 1, 2\}$. Again, our **DeepGSB-ac** reaches the same ρ_{target} despite being subject to different levels of stochasticity. This is in contrast to [15], which, due to discarding the SDE dynamics, necessitates solving PDEs on the entire state space that may be sensitive to hyperparameters. In short, our DeepGSB outperforms prior methods [14–16] by better respecting obstacles and MF interactions yet without losing convergence to ρ_{target} , and its performance remains robust across different MFGs.

4.2 High-dimensional opinion depolarization

Next, we showcase our DeepGSB in solving high-dimensional MFGs in the application of opinion dynamics [3–5], where each agent now possesses a d -dimensional opinion $x \in \mathbb{R}^d$ that evolves through the interactions with the population. In light of increasing recent attention, we consider a particular class of opinion dynamics known to yield strong *polarization* [4], *i.e.*, the agents’ opinions tend to partition into groups holding diametric views. Take the *party model* [4] for instance: Given a random information $\xi \in \mathbb{R}^d$ sampled from some distribution independent of ρ , each agent updates

⁶As stated in [16], the complexity scales *quadratically* w.r.t. the number of discretized grid points.

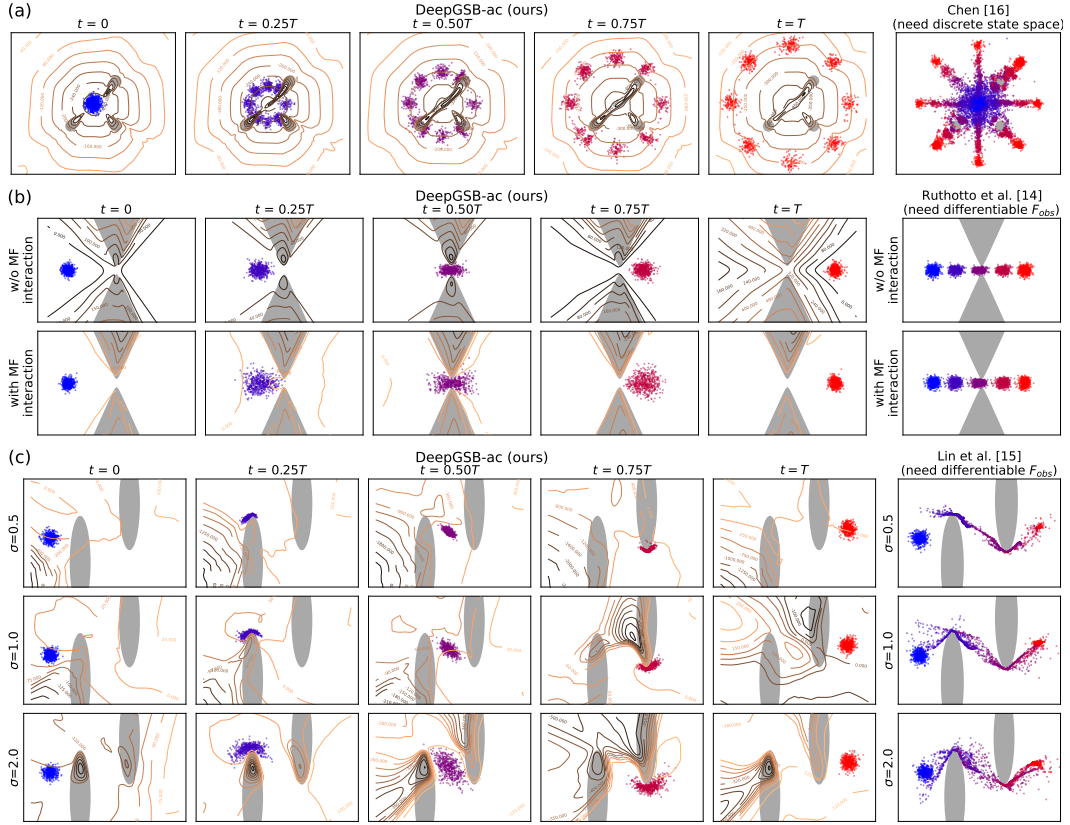


Figure 5: Simulation of the three crowd navigation MFGs, including (a) **GMM**, (b) **V-neck**, and (c) **S-tunnel**, from $t = 0$ to T . The first five columns show the population snapshots, each with a different color, guided by our **DeepGSB-ac**, whereas the sixth (rightmost) column overlays the same population snapshots generated by existing methods [14–16]. The time-varying contours represent $Y_\theta \approx \log \Psi$ whose gradient relates to the policy via $Z = \sigma \nabla Y$. This figure is best viewed in color.

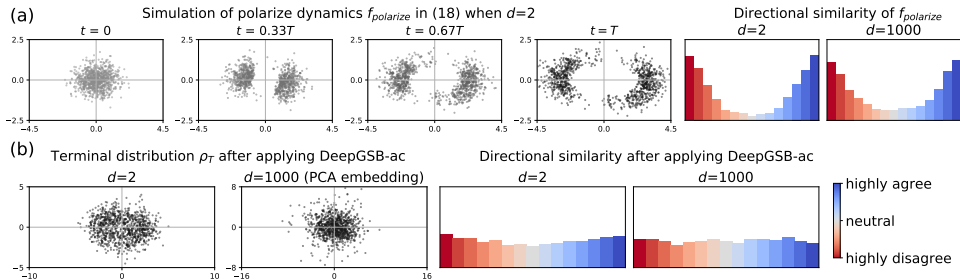


Figure 6: (a) Visualization of polarized dynamics $\bar{f}_{\text{polarize}}$ in 2- and 1000-dimensional opinion space, where the *directional similarity* [3] counts the histogram of cosine angle between pairwise opinions at the terminal distribution ρ_T . (b) **DeepGSB-ac** guides ρ_T toward moderated distributions, hence *depolarizes* the opinion dynamics. We use the first two principal components to visualize $d=1000$.

the opinion following a normalized polarize dynamic $\bar{f}_{\text{polarize}} = f_{\text{polarize}} / \|f_{\text{polarize}}\|^{\frac{1}{2}}$, where

$$f_{\text{polarize}}(x, \rho; \xi) := \mathbb{E}_{y \sim \rho} [a(x, y; \xi) \bar{y}], \quad a(x, y; \xi) := \begin{cases} 1 & \text{if } \text{sign}(\langle x, \xi \rangle) = \text{sign}(\langle y, \xi \rangle) \\ -1 & \text{otherwise} \end{cases}, \quad (18)$$

and $\bar{y} = y / \|y\|^{\frac{1}{2}}$. The *agreement* function $a(x, y; \xi)$ indicates whether the two opinions x and y agree on the information ξ . Intuitively, the dynamic in (18) suggests that the agents tend to be receptive to opinions they agree with, and antagonistic to opinions they disagree with. As shown in Fig. 6a, this behavioral assumption, also known as biased assimilation [57, 58], can easily lead to polarization.

We can apply our MFG framework (7) to this polarized base drift (18), where, starting from some weakly polarized ρ_0 , we seek a policy that compensates the polarization tendency and helps guide the opinion towards a moderated distribution ρ_{target} (assuming as Gaussian for simplicity). We consider the entropy MF interaction F_{entropy} as it encourages opinions diversity before reaching consensus. As shown in Fig. 6b, in both lower- ($d=2$) and higher- ($d=1000$) dimensions, our **DeepGSB-ac** successfully guides the opinion towards the desired distribution centered symmetrically at $\mathbf{0} \in \mathbb{R}^d$, thereby mitigates the polarization. Results of DeepGSB-c remain similar despite being more sensitive to hyperparameters; see Appendix A.5.2. We highlight these state-of-the-art results on a challenging class of MFGs that, comparing to existing methods [14, 15], consider a more difficult mean-field dynamic ($f(x, \rho)$ vs. $f(x)$) in an order of magnitude higher dimension ($d=1000$ vs. $d=100$).

4.3 Discussion

DeepGSB-ca vs. DeepGSB-c. Table 3 compares actor-critic with critic parametrizations on crowd navigation MFGs. While DeepGSB-ac typically achieves lower Wasserstein and TD errors, it seldom closes the consistency gap of $\mathcal{L}_{\text{FK}}(\theta)$, as opposed to DeepGSB-c. In practice, the results of DeepGSB-c are visually indistinguishable from DeepGSB-ac, despite the different contours of Y ; see Appendix A.5.2 for more discussions.

Table 3: Comparison of DeepGSB-ac vs. DeepGSB-c w.r.t Wasserstein distance to ρ_{target} and FBSDEs violation, in terms of TD errors and nonlinear FK, averaged over 3 runs.

MFGs	DeepGSB	$\mathcal{W}_2 \downarrow$	FBSDEs Violation \downarrow		
			$\mathcal{L}_{\text{TD}}(\phi)$	$\mathcal{L}_{\text{TD}}(\theta)$	$\mathcal{L}_{\text{FK}}(\theta)$
GMM	-ac	.27 \pm .16	9.5 \pm 2.5	7.1 \pm 0.6	5.2 \pm 1.1
	-c	.61 \pm .91	7.0 \pm 1.3	10.1 \pm 1.6	0.0 \pm 0.0
V-neck	-ac	.00 \pm .00	4.9 \pm 1.5	4.1 \pm 0.5	0.6 \pm 0.2
	-c	.01 \pm .00	8.2 \pm 0.8	8.7 \pm 1.6	0.0 \pm 0.0
S-tunnel	-ac	.01 \pm .00	25.5 \pm 2.3	28.6 \pm 3.6	2.1 \pm 0.1
	-c	.03 \pm .01	30.9 \pm 6.9	26.4 \pm 5.5	0.0 \pm 0.0

DeepGSB works with intractable ρ_{target} . While the availability of the target density ρ_{target} is a common assumption adopted in prior works [14, 15], in which ρ_{target} is involved in computing the boundary loss, in most real-world applications, ρ_{target} is seldom available. Here, we show that DeepGSB works well without knowing ρ_{target} (and ρ_0) so long as we can sample from $X_0 \sim \rho_0$ and $\bar{X}_0 \sim \rho_{\text{target}}$. This is similar to the setup of generative modeling [27]. In Fig. 7, we show that DeepGSB trained without the initial and terminal densities can converge equally well. Crucially, this is because DeepGSB relies on a variety of other mechanisms (e.g., self-consistency in single-step TD objectives and KL-matching in IPF objective) to generate equally informative gradients. This is in contrast to [14, 15] where the training signals are mostly obtained by differentiating through $D_{\text{KL}}(\rho || \rho_{\text{target}})$; consequently, their methods fail to converge in the absence of ρ_{target} .

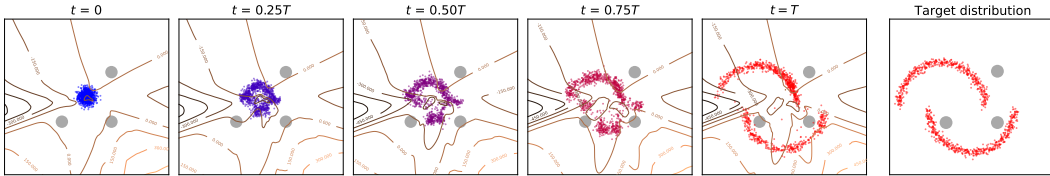


Figure 7: DeepGSB-ac trained *without* access to the initial and target distributions, i.e., without TD_0 and $\widehat{\text{TD}}_0$. In this case, we compute \mathcal{L}_{TD} with the single-step formulation in (14).

5 Conclusion and Limitation

We present **DeepGSB**, a new numerical method for solving a challenging class of MFGs with distributional boundary constraints. By generalizing prior FBSDE theory for Schrödinger Bridge to accepting mean-field interactions, we show that practical training can be achieved via an intriguing algorithmic connection to DeepRL. Our DeepGSB outperforms prior methods in crowd navigation MFGs and sets a new state-of-the-art record in depolarizing 1000-dimensional opinion MFGs.

DeepGSB is mainly developed for MFGs in *unconstrained* state spaces such as \mathbb{R}^d . Yet, it may be necessary to adopt domain-specific structures, e.g., *constrained* state spaces. Additionally, the divergence in the IPF objectives may scale unfavorably as the dimension grows. This may be mitigated by adopting a simpler regression from De Bortoli et al. [24]. We leave this as a promising future direction.

Boarder Impact

Study of Mean-Field Games (MFGs) possesses its own societal influence. Thus, as a MFG solver, DeepGSB may pose a potential impact in offering solutions to previously unsolvable MFGs under more practical settings, thereby facilitating new understanding of population behavior.

Acknowledgments and Disclosure of Funding

The authors would like to thank Yu-ting Chiang, Augustinos and Molei for their helpful supports and kind discussion. The authors would also like to thank the anonymous Reviewer A4H3 for his/her initially harsh yet constructive comments on OpenReview, which led to substantial improvements of the theoretical results during rebuttal.

References

- [1] Yves Achdou, Francisco J Buera, Jean-Michel Lasry, Pierre-Louis Lions, and Benjamin Moll. Partial differential equation models in macroeconomics. *Philosophical Transactions of the Royal Society A: Mathematical, Physical and Engineering Sciences*, 372(2028):20130397, 2014.
- [2] Yves Achdou, Jiequn Han, Jean-Michel Lasry, Pierre-Louis Lions, and Benjamin Moll. Income and wealth distribution in macroeconomics: A continuous-time approach. *The review of economic studies*, 89(1):45–86, 2022.
- [3] Simon Schweighofer, David Garcia, and Frank Schweitzer. An agent-based model of multi-dimensional opinion dynamics and opinion alignment. *Chaos: An Interdisciplinary Journal of Nonlinear Science*, 30(9):093139, 2020.
- [4] Jason Gaitonde, Jon Kleinberg, and Éva Tardos. Polarization in geometric opinion dynamics. In *Proceedings of the 22nd ACM Conference on Economics and Computation*, pages 499–519, 2021.
- [5] Jan Hązła, Yan Jin, Elchanan Mossel, and Govind Ramnarayan. A geometric model of opinion polarization. *arXiv preprint arXiv:1910.05274*, 2019.
- [6] Zhiyu Liu, Bo Wu, and Hai Lin. A mean field game approach to swarming robots control. In *2018 Annual American Control Conference (ACC)*, pages 4293–4298. IEEE, 2018.
- [7] Karthik Elamvazhuthi and Spring Berman. Mean-field models in swarm robotics: A survey. *Bioinspiration & Biomimetics*, 15(1):015001, 2019.
- [8] Yiping Lu, Chao Ma, Yulong Lu, Jianfeng Lu, and Lexing Ying. A mean-field analysis of deep resnet and beyond: Towards provable optimization via overparameterization from depth. *arXiv preprint arXiv:2003.05508*, 2020.
- [9] Kaitong Hu, Anna Kazeykina, and Zhenjie Ren. Mean-field langevin system, optimal control and deep neural networks. *arXiv preprint arXiv:1909.07278*, 2019.
- [10] E Weinan, Jiequn Han, and Qianxiao Li. A mean-field optimal control formulation of deep learning. *arXiv preprint arXiv:1807.01083*, 2018.
- [11] Jean-Michel Lasry and Pierre-Louis Lions. Mean field games. *Japanese journal of mathematics*, 2(1):229–260, 2007.
- [12] Olivier Guéant, Jean-Michel Lasry, and Pierre-Louis Lions. Mean field games and applications. In *Paris-Princeton lectures on mathematical finance 2010*, pages 205–266. Springer, 2011.
- [13] Alain Bensoussan, Jens Frehse, Phillip Yam, et al. *Mean field games and mean field type control theory*, volume 101. Springer, 2013.
- [14] Lars Ruthotto, Stanley J Osher, Wuchen Li, Levon Nurbekyan, and Samy Wu Fung. A machine learning framework for solving high-dimensional mean field game and mean field control problems. *Proceedings of the National Academy of Sciences*, 117(17):9183–9193, 2020.

- [15] Alex Tong Lin, Samy Wu Fung, Wuchen Li, Levon Nurbekyan, and Stanley J Osher. Alternating the population and control neural networks to solve high-dimensional stochastic mean-field games. *Proceedings of the National Academy of Sciences*, 118(31), 2021.
- [16] Yongxin Chen. Density control of interacting agent systems. *arXiv preprint arXiv:2108.07342*, 2021.
- [17] Jiequn Han, Arnulf Jentzen, and E Weinan. Solving high-dimensional partial differential equations using deep learning. *Proceedings of the National Academy of Sciences*, 115(34): 8505–8510, 2018.
- [18] Ioannis Exarchos and Evangelos A Theodorou. Stochastic optimal control via forward and backward stochastic differential equations and importance sampling. *Automatica*, 87:159–165, 2018.
- [19] Marcus Pereira, Ziyi Wang, Ioannis Exarchos, and Evangelos A Theodorou. Neural network architectures for stochastic control using the nonlinear feynman-kac lemma. *arXiv preprint arXiv:1902.03986*, 2019.
- [20] René Carmona, François Delarue, and Aimé Lachapelle. Control of mckean–vlasov dynamics versus mean field games. *Mathematics and Financial Economics*, 7(2):131–166, 2013.
- [21] René Carmona and François Delarue. Mean field forward-backward stochastic differential equations. *Electronic Communications in Probability*, 18:1–15, 2013.
- [22] René Carmona and Mathieu Laurière. Convergence analysis of machine learning algorithms for the numerical solution of mean field control and games: Ii—the finite horizon case. *arXiv preprint arXiv:1908.01613*, 2019.
- [23] René Carmona and Mathieu Laurière. Convergence analysis of machine learning algorithms for the numerical solution of mean field control and games i: the ergodic case. *SIAM Journal on Numerical Analysis*, 59(3):1455–1485, 2021.
- [24] Valentin De Bortoli, James Thornton, Jeremy Heng, and Arnaud Doucet. Diffusion schrödinger bridge with applications to score-based generative modeling. *arXiv preprint arXiv:2106.01357*, 2021.
- [25] Francisco Vargas, Pierre Thodoroff, Neil D Lawrence, and Austen Lamacraft. Solving schrödinger bridges via maximum likelihood. *arXiv preprint arXiv:2106.02081*, 2021.
- [26] Gefei Wang, Yuling Jiao, Qian Xu, Yang Wang, and Can Yang. Deep generative learning via schrödinger bridge. *arXiv preprint arXiv:2106.10410*, 2021.
- [27] Tianrong Chen, Guan-Horng Liu, and Evangelos A Theodorou. Likelihood training of schrödinger bridge using forward-backward sdes theory. *arXiv preprint arXiv:2110.11291*, 2021.
- [28] Charlotte Bunne, Ya-Ping Hsieh, Marco Cuturi, and Andreas Krause. Recovering stochastic dynamics via gaussian schrödinger bridges. *arXiv preprint arXiv:2202.05722*, 2022.
- [29] Erwin Schrödinger. Sur la théorie relativiste de l’électron et l’interprétation de la mécanique quantique. In *Annales de l’institut Henri Poincaré*, volume 2, pages 269–310, 1932.
- [30] Kenneth Caluya and Abhishek Halder. Wasserstein proximal algorithms for the schrödinger bridge problem: Density control with nonlinear drift. *IEEE Transactions on Automatic Control*, 2021.
- [31] Julio Backhoff, Giovanni Conforti, Ivan Gentil, and Christian Léonard. The mean field schrödinger problem: ergodic behavior, entropy estimates and functional inequalities. *Probability Theory and Related Fields*, 178(1):475–530, 2020.
- [32] Yongxin Chen, Tryphon Georgiou, and Michele Pavon. Optimal steering of inertial particles diffusing anisotropically with losses. In *2015 American Control Conference (ACC)*, pages 1252–1257. IEEE, 2015.

- [33] Erwin Schrödinger. *Über die umkehrung der naturgesetze*. Verlag der Akademie der Wissenschaften in Kommission bei Walter De Gruyter u . . . , 1931.
- [34] Christian Léonard. From the schrödinger problem to the monge–kantorovich problem. *Journal of Functional Analysis*, 262(4):1879–1920, 2012.
- [35] Christian Léonard. A survey of the schrödinger problem and some of its connections with optimal transport. *arXiv preprint arXiv:1308.0215*, 2013.
- [36] Michele Pavon and Anton Wakolbinger. On free energy, stochastic control, and schrödinger processes. In *Modeling, Estimation and Control of Systems with Uncertainty*, pages 334–348. Springer, 1991.
- [37] Paolo Dai Pra. A stochastic control approach to reciprocal diffusion processes. *Applied mathematics and Optimization*, 23(1):313–329, 1991.
- [38] Francisco Vargas. Machine-learning approaches for the empirical schrödinger bridge problem. Technical report, University of Cambridge, Computer Laboratory, 2021.
- [39] Jean-David Benamou, Guillaume Carlier, Marco Cuturi, Luca Nenna, and Gabriel Peyré. Iterative bregman projections for regularized transportation problems. *SIAM Journal on Scientific Computing*, 37(2):A1111–A1138, 2015.
- [40] Solomon Kullback. Probability densities with given marginals. *The Annals of Mathematical Statistics*, 39(4):1236–1243, 1968.
- [41] Qinsheng Zhang and Yongxin Chen. Path integral sampler: a stochastic control approach for sampling. *arXiv preprint arXiv:2111.15141*, 2021.
- [42] Eberhard Hopf. The partial differential equation $u_t + u u_x = \mu x x$. *Communications on Pure and Applied mathematics*, 3(3):201–230, 1950.
- [43] Julian D Cole. On a quasi-linear parabolic equation occurring in aerodynamics. *Quarterly of applied mathematics*, 9(3):225–236, 1951.
- [44] Jiongmin Yong and Xun Yu Zhou. *Stochastic controls: Hamiltonian systems and HJB equations*, volume 43. Springer Science & Business Media, 1999.
- [45] Magdalena Kobylanski. Backward stochastic differential equations and partial differential equations with quadratic growth. *Annals of probability*, pages 558–602, 2000.
- [46] Kiyosi Itô. *On stochastic differential equations*, volume 4. American Mathematical Soc., 1951.
- [47] Richard Bellman. The theory of dynamic programming. Technical report, Rand corp santa monica ca, 1954.
- [48] Emanuel Todorov. Efficient computation of optimal actions. *Proceedings of the national academy of sciences*, 106(28):11478–11483, 2009.
- [49] Michael Lutter, Shie Mannor, Jan Peters, Dieter Fox, and Animesh Garg. Value iteration in continuous actions, states and time. *arXiv preprint arXiv:2105.04682*, 2021.
- [50] Lingheng Meng, Rob Gorbet, and Dana Kulić. The effect of multi-step methods on overestimation in deep reinforcement learning. In *2020 25th International Conference on Pattern Recognition (ICPR)*, pages 347–353. IEEE, 2021.
- [51] Harm van Seijen. Effective multi-step temporal-difference learning for non-linear function approximation. *arXiv preprint arXiv:1608.05151*, 2016.
- [52] Matteo Hessel, Joseph Modayil, Hado Van Hasselt, Tom Schaul, Georg Ostrovski, Will Dabney, Dan Horgan, Bilal Piot, Mohammad Azar, and David Silver. Rainbow: Combining improvements in deep reinforcement learning. In *Thirty-second AAAI conference on artificial intelligence*, 2018.

- [53] Volodymyr Mnih, Koray Kavukcuoglu, David Silver, Alex Graves, Ioannis Antonoglou, Daan Wierstra, and Martin Riedmiller. Playing atari with deep reinforcement learning. *arXiv preprint arXiv:1312.5602*, 2013.
- [54] Timothy P Lillicrap, Jonathan J Hunt, Alexander Pritzel, Nicolas Heess, Tom Erez, Yuval Tassa, David Silver, and Daan Wierstra. Continuous control with deep reinforcement learning. *arXiv preprint arXiv:1509.02971*, 2015.
- [55] John Schulman, Sergey Levine, Pieter Abbeel, Michael Jordan, and Philipp Moritz. Trust region policy optimization. In *International conference on machine learning*, pages 1889–1897, 2015.
- [56] Ilya Loshchilov and Frank Hutter. Decoupled weight decay regularization. *arXiv preprint arXiv:1711.05101*, 2017.
- [57] Charles G Lord, Lee Ross, and Mark R Lepper. Biased assimilation and attitude polarization: The effects of prior theories on subsequently considered evidence. *Journal of personality and social psychology*, 37(11):2098, 1979.
- [58] Pranav Dandekar, Ashish Goel, and David T Lee. Biased assimilation, homophily, and the dynamics of polarization. *Proceedings of the National Academy of Sciences*, 110(15):5791–5796, 2013.
- [59] Etienne Pardoux and Shige Peng. Backward stochastic differential equations and quasilinear parabolic partial differential equations. In *Stochastic partial differential equations and their applications*, pages 200–217. Springer, 1992.
- [60] Balint Negyesi, Kristoffer Andersson, and Cornelis W Oosterlee. The one step malliavin scheme: new discretization of bsdes implemented with deep learning regressions. *arXiv preprint arXiv:2110.05421*, 2021.
- [61] Qianxiao Li and Shuji Hao. An optimal control approach to deep learning and applications to discrete-weight neural networks. In *International Conference on Machine Learning*, pages 2985–2994. PMLR, 2018.
- [62] Guan-Horng Liu, Tianrong Chen, and Evangelos A Theodorou. Ddpnpt: Differential dynamic programming neural optimizer. In *International Conference on Learning Representations*, 2021.
- [63] Guan-Horng Liu, Tianrong Chen, and Evangelos A Theodorou. Second-order neural ode optimizer. In *Advances in Neural Information Processing Systems*, 2021.
- [64] Yang Song, Jascha Sohl-Dickstein, Diederik P Kingma, Abhishek Kumar, Stefano Ermon, and Ben Poole. Score-based generative modeling through stochastic differential equations. *arXiv preprint arXiv:2011.13456*, 2020.
- [65] Edward Nelson. *Dynamical theories of Brownian motion*, volume 106. Princeton university press, 2020.
- [66] Brian DO Anderson. Reverse-time diffusion equation models. *Stochastic Processes and their Applications*, 12(3):313–326, 1982.
- [67] Grigorios A Pavliotis. *Stochastic processes and applications: diffusion processes, the Fokker-Planck and Langevin equations*, volume 60. Springer, 2014.
- [68] Yang Song, Conor Durkan, Iain Murray, and Stefano Ermon. Maximum likelihood training of score-based diffusion models. *arXiv e-prints*, pages arXiv–2101, 2021.
- [69] Chin-Wei Huang, Jae Hyun Lim, and Aaron Courville. A variational perspective on diffusion-based generative models and score matching. *arXiv preprint arXiv:2106.02808*, 2021.
- [70] Stefan Elfving, Eiji Uchibe, and Kenji Doya. Sigmoid-weighted linear units for neural network function approximation in reinforcement learning. *Neural Networks*, 107:3–11, 2018.
- [71] Adam Paszke, Sam Gross, Soumith Chintala, Gregory Chanan, Edward Yang, Zachary DeVito, Zeming Lin, Alban Desmaison, Luca Antiga, and Adam Lerer. Automatic differentiation in pytorch. 2017.

A Appendix

A.1	Summary of Abbreviation and Notation	15
A.2	Review of Nonlinear FK Lemma and SB-FBSDE	15
A.3	Proofs in Main Paper	17
A.3.1	Preliminary	17
A.3.2	Proof of Lemma 1	18
A.3.3	Proof of Theorem 2	19
A.3.4	Proof of Proposition 3	21
A.3.5	Proof of Proposition 4	21
A.4	Additional Derivations & Remarks in Sec. 3 and 4	23
A.4.1	Hopf-Cole transform	23
A.4.2	Remarks on convergence	23
A.4.3	Functional derivative of MF potential functions	24
A.5	Experiment Details	24
A.5.1	Setup	24
A.5.2	Additional experiments	26

A.1 Summary of Abbreviation and Notation

Table 4: Abbreviation.

MFGs	Mean-Field Games
SB	Schrödinger Bridge
DeepRL	Deep Reinforcement Learning
PDEs	Partial Differential Equations
HJB	Hamilton-Jacobi-Bellman
FP	Fokker-Plank
SDEs	Stochastic Differential Equations
FBSDEs	Forward-Backward SDEs
IPF	Iterative Proportional Fitting
MF interaction	Mean-field interaction
nonlinear FK	nonlinear Feynman-Kac
TD	Temporal Difference

Table 5: Notation.

t	time coordinate
s	reversed time coordinate
$u(t, x)$	value function
$\rho(t, x)$	marginal distribution
$\rho_0, \rho_{\text{target}}$	initial/target distributions
H	Hamiltonian function
F	MF interaction function
f	MF base drift
σ	diffusion scaler
$(\Psi, \widehat{\Psi})$	solution to SB PDEs
(Y, Z)	nonlinear FK of Ψ
$(\widehat{Y}, \widehat{Z})$	nonlinear FK of $\widehat{\Psi}$
TD_s	TD target for Y_s
$\widehat{\text{TD}}_t$	TD target for \widehat{Y}_t
θ	Parameter of Y (and Z)
ϕ	Parameter of \widehat{Y} (and \widehat{Z})

A.2 Review of Nonlinear FK Lemma and SB-FBSDE

Lemma 5 (Nonlinear Feynman-Kac Lemma [18, 44, 45]). *Let $v \equiv v(x, t)$ be a function that is twice continuously differentiable in $x \in \mathbb{R}^d$ and once differentiable in $t \in [0, T]$, i.e., $v \in C^{2,1}(\mathbb{R}^d, [0, T])$.*

Consider the following second-order parabolic PDE,

$$\frac{\partial v}{\partial t} + \frac{1}{2} \text{Tr}(\nabla^2 v G(x, t) G(x, t)^\top) + \nabla v^\top f(x, t) + h(x, v, G(x, t)^\top \nabla v, t) = 0, \quad v(T, x) = \varphi(x), \quad (19)$$

where ∇^2 denotes the Hessian operator w.r.t. x and the functions f , G , h , and φ satisfy proper regularity conditions. Specifically, (i) f , G , h , and φ are continuous, (ii) $f(x, t)$ and $G(x, t)$ are uniformly Lipschitz in x , and (iii) $h(x, y, z, t)$ satisfies quadratic growth condition in z . Then, (19) exists a unique solution v such that the following stochastic representation (known as the nonlinear Feynman-Kac transformation) holds:

$$Y_t = v(X_t, t), \quad Z_t = G(X_t, t)^\top \nabla v(X_t, t), \quad (20)$$

where (X_t, Y_t, Z_t) are the unique adapted solutions to the following FBSDEs:

$$\begin{aligned} dX_t &= f(X_t, t)dt + G(X_t, t)dW_t, & X_0 &= x_0, \\ dY_t &= -h(X_t, Y_t, Z_t, t)dt + Z_t^\top dW_t, & Y_T &= \varphi(X_T). \end{aligned} \quad (21)$$

The original deterministic PDE solution $v(x, t)$ can be recovered by taking conditional expectations:

$$\mathbb{E}[Y_t | X_t = x] = v(x, t), \quad \mathbb{E}[Z_t | X_t = x] = G(x, t)^\top \nabla v(x, t).$$

Lemma 5 establishes an intriguing connection between a certain class of (nonlinear) PDEs in (19) and FBSDEs (21) via the nonlinear FK transformation (20). In this work, we adopt a simpler diffusion $G(x, t) := \sigma$ as a time-invariant scalar but note that our derivation can be extended to more general cases straightforwardly.

Viscosity solution. Lemma 5 can be extended to viscosity solutions when the classical solution does not exist. In which case, we will have $v(x, t) = \lim_{\epsilon \rightarrow \infty} v^\epsilon(x, t)$ converge uniformly in (x, t) over a compact set, where $v^\epsilon(x, t)$ is the classical solution to (19) with $(f_\epsilon, G_\epsilon, h_\epsilon, \varphi_\epsilon)$ converge uniformly toward (f, G, h, φ) over the compact set; see [18, 59, 60] for a complete discussion.

SB-FBSDE [27]. SB-FBSDE is a new class of generative models that, inspiring by the recent advance of understanding deep learning through the optimal control perspective [61–63], adopts Lemma 5 to generalize the score-based diffusion models. Since the PDEs $(\frac{\partial \Psi}{\partial t}, \frac{\partial \hat{\Psi}}{\partial t})$ appearing in the vanilla SB (4) are both of the parabolic form (19), one can apply Lemma 5 and derive the corresponding nonlinear generators h . This, as shown in SB-FBSDE [27], leads to the following FBSDEs:

$$\begin{cases} dX_t = (f_t + \sigma Z_t) dt + \sigma dW_t & (22a) \\ dY_t = \frac{1}{2} \|Z_t\|^2 dt + Z_t^\top dW_t & (22b) \\ d\hat{Y}_t = \left(\frac{1}{2} \|\hat{Z}_t\|^2 + \nabla \cdot (\sigma \hat{Z}_t - f_t) + \hat{Z}_t^\top Z_t \right) dt + \hat{Z}_t^\top dW_t & (22c) \end{cases}$$

Further, the nonlinear FK transformation reads

$$\begin{aligned} Y_t &= \log \Psi(X_t, t), & Z_t &= \sigma \nabla \log \Psi(X_t, t), \\ \hat{Y}_t &= \log \hat{\Psi}(X_t, t), & \hat{Z}_t &= \sigma \nabla \log \hat{\Psi}(X_t, t), \end{aligned}$$

which immediately suggests that

$$\mathbb{E}[Y_t | X_t = x] = \log \Psi(x, t), \quad \mathbb{E}[\hat{Y}_t | X_t = x] = \log \hat{\Psi}(x, t). \quad (23)$$

It can be readily seen that (22) is a special case of our Theorem 2 when the MF interaction $F(x, \rho)$, which plays a crucial role in MFGs, vanishes. Since SB-FBSDE was primarily developed in the context of generative modeling [64], its training relies on computing the log-likelihood at the boundaries. These log-likelihoods can be obtained by noticing that $\log \rho(x, t) = \mathbb{E}[Y_t + \hat{Y}_t | X_t = x]$, as implied by (23) and (8). When $\hat{Z}_\phi(X_t, t) \approx \hat{Z}_t$ and $Z_\theta(\bar{X}_s, s) \approx Z_s$, the training objectives of SB-FBSDE can be computed as the parametrized variational lower-bounds:

$$\log \rho_0(\phi; x) \geq \mathcal{L}_{\text{IPF}}(\phi) := \mathbb{E}[Y_t^\theta + \hat{Y}_t^\phi | X_t = x, t = 0] = \int_t \mathbb{E} \left[dY_t^\theta + d\hat{Y}_t^\phi | X_0 = x \right], \quad (24a)$$

$$\log \rho_T(\theta; x) \geq \mathcal{L}_{\text{IPF}}(\theta) := \mathbb{E}[Y_s^\theta + \hat{Y}_s^\phi | \bar{X}_s = x, s = 0] = \int_s \mathbb{E} \left[dY_s^\theta + d\hat{Y}_s^\phi | \bar{X}_0 = x \right]. \quad (24b)$$

Invoking (22) to expand the *r.h.s.* of (24) leads to the expression in (6):

$$\begin{aligned}\mathcal{L}_{\text{IPF}}(\theta) &= \int_0^T \mathbb{E}_{(3b)} \left[\frac{1}{2} \|Z_\theta(\bar{X}_s, s)\|_2^2 + Z_\theta(\bar{X}_s, s)^\top \widehat{Z}_\phi(\bar{X}_s, s) + \nabla \cdot (\sigma Z_\theta(\bar{X}_s, s) + f) \right] ds, \\ \mathcal{L}_{\text{IPF}}(\phi) &= \int_0^T \mathbb{E}_{(3a)} \left[\frac{1}{2} \|\widehat{Z}_\phi(X_t, t)\|_2^2 + \widehat{Z}_\phi(X_t, t)^\top Z_\theta(X_t, t) + \nabla \cdot (\sigma \widehat{Z}_\phi(X_t, t) - f) \right] dt.\end{aligned}$$

Since (24) concern only the integration over the expectations, *i.e.*, $\int \mathbb{E}[dY + d\widehat{Y}]$, the solutions (Y_t, \widehat{Y}_t) to the SDEs (22b, 22c) were *never* computed explicitly in SB-FBSDE, This is in contrast to our DeepGSB, which, crucially, requires computing (Y_t, \widehat{Y}_t) explicitly and regress their values with TD objectives, so that the stochastic dynamics of dY and $d\widehat{Y}$ are respectively respected.

A.3 Proofs in Main Paper

Throughout this section, we will denote the parameterized forward and backward SDEs by

$$dX_t^\theta = (f_t + \sigma Z_\theta(X_t^\theta, t)) dt + \sigma dW_t, \quad (25a)$$

$$d\bar{X}_s^\phi = \left(-f_s + \sigma \widehat{Z}_\phi(\bar{X}_s^\phi, t) \right) ds + \sigma dW_s, \quad (25b)$$

and denote their time-marginal densities respectively as q^θ and q^ϕ .

A.3.1 Preliminary

We first restate some useful lemmas that will appear in the proceeding proofs.

Lemma 6 (Itô formula [46]). *Let X_t be the solution to the Itô SDE:*

$$dX_t = f(X_t, t)dt + \sigma(X_t, t)dW_t.$$

Then, the stochastic process $v(X_t, t)$, where $v \in C^{2,1}(\mathbb{R}^d, [0, T])$, is also an Itô process satisfying

$$dv(X_t, t) = \frac{\partial v(X_t, t)}{\partial t} dt + \left[\nabla v(X_t, t)^\top f + \frac{1}{2} \text{Tr} [\sigma^\top \nabla^2 v(X_t, t) \sigma] \right] dt + [\nabla v(X_t, t)^\top \sigma] dW_t. \quad (26)$$

Lemma 7. *The following equality holds at any point $x \in \mathbb{R}^n$ such that $p(x) \neq 0$.*

$$\frac{1}{p(x)} \Delta p(x) = \|\nabla \log p(x)\|^2 + \Delta \log p(x)$$

Proof. $\frac{1}{p(x)} \Delta p(x) = \frac{1}{p(x)} \nabla \cdot \nabla p(x) = \frac{1}{p(x)} \nabla \cdot (p(x) \nabla \log p(x))$. Applying chain rule to the divergence yields the desired result. \square

Lemma 8 (Vargas [38], Proposition 1, Sec 6.3.1).

$$d \log q_t^\phi = \left[\nabla \cdot (\sigma \widehat{Z}_\phi - f_t) + \sigma (Z_\theta + \widehat{Z}_\phi)^\top \nabla \log q_t^\phi - \frac{1}{2} \|\sigma \nabla \log q_t^\phi\|^2 \right] dt + \sigma \nabla \log q_t^\phi^\top dW_t.$$

Proof. Invoking Ito lemma w.r.t. the parameterized forward SDE (25a),

$$d \log q_t^\phi = \left[\frac{\partial \log q_t^\phi}{\partial t} + \nabla \log q_t^\phi^\top (f_t + \sigma Z_\theta) + \frac{\sigma^2}{2} \Delta \log q_t^\phi \right] dt + \sigma \nabla \log q_t^\phi^\top dW_t,$$

where $\frac{\partial \log q_t^\phi}{\partial t}$ obeys (see Eq 13.4 in Nelson [65]):

$$\begin{aligned}-\frac{\partial \log q_t^\phi}{\partial t} &= -\nabla \cdot \left((\sigma \widehat{Z}_\phi - f_t) q_t^\phi \right) + \frac{\sigma^2}{2} \Delta q_t^\phi \\ \Rightarrow \frac{\partial \log q_t^\phi}{\partial t} &= \nabla \cdot (\sigma \widehat{Z}_\phi - f_t) + (\sigma \widehat{Z}_\phi - f_t)^\top \nabla \log q_t^\phi - \frac{\sigma^2 \Delta q_t^\phi}{2q_t^\phi}.\end{aligned}$$

Substituting the above relation yields the desired results. \square

Proposition 9 (Vargas [38], Proposition 1 in Sec 6.3.1).

$$D_{\text{KL}}(q^\theta || q^\phi) = \int_0^T \mathbb{E}_{q_t^\theta} \left[\frac{1}{2} \|\widehat{Z}_\phi + Z_\theta\|^2 + \nabla \cdot (\sigma \widehat{Z}_\phi - f_t) \right] dt + \mathbb{E}_{q_0^\theta} [\log \rho_0] - \mathbb{E}_{q_T^\theta} [\log \rho_{\text{target}}]$$

Proof. Recall that the parametrized backward SDE (25b) can be reversed [64, 66] as

$$d\bar{X}_t^\phi = \left(f_t - \sigma \widehat{Z}_\phi(\bar{X}_t^\phi, t) + \sigma^2 \nabla \log q^\phi(\bar{X}_t^\phi, t) \right) dt + \sigma dW_t.$$

Then, we have

$$\begin{aligned} & D_{\text{KL}}(q^\theta || q^\phi) \\ &= \int_0^T \mathbb{E}_{q_t^\theta} \left[\frac{1}{2} \|\widehat{Z}_\phi + Z_\theta - \sigma \nabla \log q_t^\phi\|^2 \right] dt + D_{\text{KL}}(\rho_0 || q_{t=0}^\phi) \\ &= \int_0^T \mathbb{E}_{q_t^\theta} \left[\frac{1}{2} \|\widehat{Z}_\phi + Z_\theta\|^2 - \sigma (\widehat{Z}_\phi + Z_\theta)^\top \nabla \log q_t^\phi + \frac{1}{2} \|\sigma \nabla \log q_t^\phi\|^2 \right] dt + D_{\text{KL}}(\rho_0 || q_{t=0}^\phi) \\ &\stackrel{(*)}{=} \int_0^T \mathbb{E}_{q_t^\theta} \left[\frac{1}{2} \|\widehat{Z}_\phi + Z_\theta\|^2 + \nabla \cdot (\sigma \widehat{Z}_\phi - f_t) \right] dt - \mathbb{E}_{q^\theta} \left[\int_0^T d \log q_t^\phi \right] + D_{\text{KL}}(\rho_0 || q_{t=0}^\phi) \\ &= \int_0^T \mathbb{E}_{q_t^\theta} \left[\frac{1}{2} \|\widehat{Z}_\phi + Z_\theta\|^2 + \nabla \cdot (\sigma \widehat{Z}_\phi - f_t) \right] dt + \mathbb{E}_{q_0^\theta} [\log \rho_0] - \mathbb{E}_{q_T^\theta} [\log \rho_{\text{target}}], \end{aligned}$$

where (*) is due to Lemma 8. \square

A.3.2 Proof of Lemma 1

Proof. Substituting $\mathcal{L}_{\text{IPF}}(\phi)$ into Proposition 9 and dropping all terms independent of ϕ readily yields $D_{\text{KL}}(q^\theta || q^\phi) \propto \mathcal{L}_{\text{IPF}}(\phi)$. A similar relation can be derived between $D_{\text{KL}}(q^\phi || q^\theta)$. \square

Remark (an alternative simpler proof). Suppose (Z_θ, q^θ) and $(\widehat{Z}_\phi, q^\phi)$ satisfy proper regularity such that $\forall t, s \in [0, T], \exists k > 0 : q^\theta(x, t) = \mathcal{O}(\exp^{-\|x\|_k^2}), q^\phi(x, s) = \mathcal{O}(\exp^{-\|x\|_k^2})$ as $x \rightarrow \infty$. Then, an alternative proof using integration by part goes as follows: Recall that the parametrized forward SDE in (25a) can be reversed [64, 66] as

$$dX_s^\theta = (-f_s - \sigma Z_\theta(X_s^\theta, s) + \sigma^2 \nabla \log q^\theta(X_s^\theta, s)) ds + \sigma dW_s.$$

Then, the KL divergence can be computed as

$$\begin{aligned} & D_{\text{KL}}(q^\theta || q^\phi) \\ &\stackrel{(*)}{=} \mathbb{E}_{q^\theta} \left[\int_0^T \frac{1}{2\sigma^2} \|\sigma \widehat{Z}_\phi + \sigma Z_\theta - \sigma^2 \nabla \log q_s^\theta\|^2 ds \right] + D_{\text{KL}}(q_{s=0}^\theta || \rho_{\text{target}}) \tag{27} \\ &= \int_0^T \mathbb{E}_{q_s^\theta} \left[\frac{1}{2} \|\widehat{Z}_\phi + Z_\theta\|^2 - \sigma (\widehat{Z}_\phi + Z_\theta)^\top \nabla \log q_s^\theta + \frac{1}{2} \|\sigma \nabla \log q_s^\theta\|^2 \right] ds + D_{\text{KL}}(q_0^\theta || \rho_{\text{target}}) \\ &= \int_0^T \mathbb{E}_{q_s^\theta} \left[\frac{1}{2} \|\widehat{Z}_\phi\|^2 + \widehat{Z}_\phi^\top Z_\theta - \sigma \widehat{Z}_\phi^\top \nabla \log q_s^\theta \right] ds + \mathcal{O}(1) \\ &\stackrel{(**)}{=} \int_0^T \mathbb{E}_{q_s^\theta} \left[\frac{1}{2} \|\widehat{Z}_\phi\|^2 + \widehat{Z}_\phi^\top Z_\theta + \sigma \nabla \cdot \widehat{Z}_\phi \right] ds + \mathcal{O}(1), \\ &\propto \mathcal{L}_{\text{IPF}}(\phi) \end{aligned}$$

where (*) is due to the Girsanov's Theorem [67] and (**) is due to **integration by parts**. $\mathcal{O}(1)$ collects terms independent of ϕ . Notice that the boundary terms vanish due to the additional regularity assumptions on q^θ and q^ϕ . Similar transformations have been adopted in *e.g.*, Theorem 1 in Song et al. [68] or Theorem 3 in Huang et al. [69].

A.3.3 Proof of Theorem 2

Proof. Apply the Itô formula to $v := \log \Psi(X_t, t)$, where X_t follows (3a),

$$d \log \Psi = \frac{\partial \log \Psi}{\partial t} dt + \left[\nabla \log \Psi^\top (f + \sigma^2 \nabla \log \Psi) + \frac{\sigma^2}{2} \Delta \log \Psi \right] dt + \sigma \nabla \log \Psi^\top dW_t,$$

and notice that the PDE of $\frac{\partial \log \Psi}{\partial t}$ obeys

$$\frac{\partial \log \Psi}{\partial t} = \frac{1}{\Psi} \left(-\nabla \Psi^\top f - \frac{\sigma^2}{2} \Delta \Psi + F \Psi \right) = -\nabla \log \Psi^\top f - \frac{\sigma^2}{2} \|\nabla \log \Psi\|^2 - \frac{\sigma^2}{2} \Delta \log \Psi + F.$$

This yields

$$d \log \Psi = \left[\frac{1}{2} \|\sigma \nabla \log \Psi\|^2 + F \right] dt + \sigma \nabla \log \Psi^\top dW_t. \quad (28)$$

Now, apply the same Itô formula by instead substituting $v := \log \widehat{\Psi}(X_t, t)$, where X_t follows (3a),

$$d \log \widehat{\Psi} = \frac{\partial \log \widehat{\Psi}}{\partial t} dt + \left[\nabla \log \widehat{\Psi}^\top (f + \sigma^2 \nabla \log \Psi) + \frac{\sigma^2}{2} \Delta \log \widehat{\Psi} \right] dt + \sigma \nabla \log \widehat{\Psi}^\top dW_t,$$

and notice that the PDE of $\frac{\partial \log \widehat{\Psi}}{\partial t}$ obeys

$$\begin{aligned} \frac{\partial \log \widehat{\Psi}}{\partial t} &= \frac{1}{\widehat{\Psi}} \left(-\nabla \cdot (\widehat{\Psi} f) + \frac{\sigma^2}{2} \Delta \widehat{\Psi} - F \widehat{\Psi} \right) \\ &= -\nabla \log \widehat{\Psi}^\top f - \nabla \cdot f + \frac{\sigma^2}{2} \|\nabla \log \widehat{\Psi}\|^2 + \frac{\sigma^2}{2} \Delta \log \widehat{\Psi} - F. \end{aligned}$$

This yields

$$\begin{aligned} d \log \widehat{\Psi} &= \left[-\nabla \cdot f + \frac{\sigma^2}{2} \|\nabla \log \widehat{\Psi}\|^2 + \sigma^2 \nabla \log \widehat{\Psi}^\top \nabla \log \Psi + \sigma^2 \Delta \log \widehat{\Psi} - F \right] dt + \sigma \nabla \log \widehat{\Psi}^\top dW_t \\ &= \left[\nabla \cdot (\sigma^2 \nabla \log \widehat{\Psi} - f) + \frac{\sigma^2}{2} \|\nabla \log \widehat{\Psi}\|^2 + \sigma^2 \nabla \log \widehat{\Psi}^\top \nabla \log \Psi - F \right] dt + \sigma \nabla \log \widehat{\Psi}^\top dW_t. \end{aligned} \quad (29)$$

Finally, with the nonlinear FK transformation in (10), *i.e.*,

$$\begin{aligned} Y_t &\equiv Y(X_t, t) = \log \Psi(X_t, t), & Z_t &\equiv Z(X_t, t) = \sigma \nabla \log \Psi(X_t, t), \\ \widehat{Y}_t &\equiv \widehat{Y}(X_t, t) = \log \widehat{\Psi}(X_t, t), & \widehat{Z}_t &\equiv \widehat{Z}(X_t, t) = \sigma \nabla \log \widehat{\Psi}(X_t, t), \end{aligned}$$

we can rewrite (3a, 28, 29) as the FBSDEs system in (11).

$$\begin{aligned} dX_t &= (f_t + \sigma Z_t) dt + \sigma dW_t \\ dY_t &= \left[\frac{1}{2} \|Z_t\|^2 + F_t \right] dt + Z_t^\top dW_t \\ d\widehat{Y}_t &= \left[\frac{1}{2} \|\widehat{Z}_t\|^2 + \widehat{Z}_t^\top Z_t + \nabla \cdot (\sigma \widehat{Z}_t - f_t) - F_t \right] dt + \widehat{Z}_t^\top dW_t \end{aligned}$$

where

$$f_t := f(X_t, \exp(Y_t + \widehat{Y}_t)), \quad F_t := F(X_t, \exp(Y_t + \widehat{Y}_t)).$$

Derivation of the second FBSDEs system in (12) follows a similar flow, except that we need to rebase the PDEs (9) to the “reversed” time coordinate $s := T - t$. This can be done by reformulating the HJB and FP PDEs in (7) under the s coordinate, then applying the following Hopf-Cole transform:

$$\widehat{\Psi}(x, s) := \exp(-u(x, s)), \quad \Psi(x, s) := \rho(x, s) \exp(u(x, s)). \quad (31)$$

Notice that we flip the role of $\widehat{\Psi}(x, s)$ and $\Psi(x, s)$ as the former now relates to the policy appearing in (3b). Omitting the computation similar to Appendix A.4.1, we arrive at the following:

$$\begin{cases} \frac{\partial \widehat{\Psi}(x, s)}{\partial s} = \nabla \widehat{\Psi}^\top f - \frac{1}{2} \sigma^2 \Delta \widehat{\Psi} + F \widehat{\Psi} \\ \frac{\partial \Psi(x, s)}{\partial s} = \nabla \cdot (\Psi f) + \frac{1}{2} \sigma^2 \Delta \Psi - F \Psi \end{cases} \quad \text{s.t.} \quad \begin{cases} \widehat{\Psi}(\cdot, 0) \Psi(\cdot, 0) = \rho_{\text{target}} \\ \widehat{\Psi}(\cdot, T) \Psi(\cdot, T) = \rho_0 \end{cases}. \quad (32)$$

Apply the Itô formula to $v := \log \Psi(\bar{X}_s, s)$, where \bar{X}_s evolves along the reversed SDE (3b).

$$d \log \Psi = \frac{\partial \log \Psi}{\partial s} ds + \left[\nabla \log \Psi^\top (-f + \sigma^2 \nabla \log \widehat{\Psi}) + \frac{\sigma^2}{2} \Delta \log \Psi \right] ds + \sigma \nabla \log \Psi^\top dW_s,$$

and notice that the PDE of $\frac{\partial \log \Psi}{\partial s}$ now obeys

$$\begin{aligned} \frac{\partial \log \Psi}{\partial s} &= \frac{1}{\Psi} \left(\nabla \cdot (\Psi f) + \frac{\sigma^2}{2} \Delta \Psi - F \Psi \right) \\ &= \nabla \log \Psi^\top f + \nabla \cdot f + \frac{\sigma^2}{2} \|\nabla \log \Psi\|^2 + \frac{\sigma^2}{2} \Delta \log \Psi - F. \end{aligned}$$

This yields

$$\begin{aligned} d \log \Psi &= \left[\nabla \cdot f + \frac{\sigma^2}{2} \|\nabla \log \Psi\|^2 + \sigma^2 \nabla \log \Psi^\top \nabla \log \widehat{\Psi} + \sigma^2 \Delta \log \Psi - F \right] ds + \sigma \nabla \log \Psi^\top dW_s \\ &= \left[\nabla \cdot (f + \sigma^2 \nabla \log \Psi) + \frac{\sigma^2}{2} \|\nabla \log \Psi\|^2 + \sigma^2 \nabla \log \Psi^\top \nabla \log \widehat{\Psi} - F \right] ds + \sigma \nabla \log \Psi^\top dW_s. \end{aligned} \quad (33)$$

Similarly, apply the Itô formula to $v := \log \widehat{\Psi}(\bar{X}_s, s)$, where \bar{X}_s follows the same reversed SDE (3b).

$$d \log \widehat{\Psi} = \frac{\partial \log \widehat{\Psi}}{\partial s} ds + \left[\nabla \log \widehat{\Psi}^\top (-f + \sigma^2 \nabla \log \widehat{\Psi}) + \frac{\sigma^2}{2} \Delta \log \widehat{\Psi} \right] ds + \sigma \nabla \log \widehat{\Psi}^\top dW_s,$$

and notice that the PDE of $\frac{\partial \log \widehat{\Psi}}{\partial s}$ obeys

$$\frac{\partial \log \widehat{\Psi}}{\partial s} = \frac{1}{\widehat{\Psi}} \left(\nabla \widehat{\Psi}^\top f - \frac{\sigma^2}{2} \Delta \widehat{\Psi} + F \widehat{\Psi} \right) = \nabla \log \widehat{\Psi}^\top f - \frac{\sigma^2}{2} \|\nabla \log \widehat{\Psi}\|^2 - \frac{\sigma^2}{2} \Delta \log \widehat{\Psi} + F.$$

This yields

$$d \log \widehat{\Psi} = \left[\frac{1}{2} \|\sigma \nabla \log \widehat{\Psi}\|^2 + F \right] ds + \sigma \nabla \log \widehat{\Psi}^\top dW_s. \quad (34)$$

Finally, with a nonlinear FK transformation similar to (10),

$$\begin{aligned} Y_s &\equiv Y(\bar{X}_s, s) = \log \Psi(\bar{X}_s, s), & Z_s &\equiv Z(\bar{X}_s, s) = \sigma \nabla \log \Psi(\bar{X}_s, s), \\ \widehat{Y}_s &\equiv \widehat{Y}(\bar{X}_s, s) = \log \widehat{\Psi}(\bar{X}_s, s), & \widehat{Z}_s &\equiv \widehat{Z}(\bar{X}_s, s) = \sigma \nabla \log \widehat{\Psi}(\bar{X}_s, s), \end{aligned} \quad (35)$$

we can rewrite (3b, 33, 34) as the second FBSDEs system in (12).

$$\begin{aligned} d\bar{X}_s &= \left(-f_s + \sigma \widehat{Z}_s \right) ds + \sigma dW_s \\ dY_s &= \left(\frac{1}{2} \|Z_s\|^2 + \nabla \cdot (\sigma Z_s + f_s) + Z_s^\top \widehat{Z}_s - F_s \right) ds + Z_s^\top dW_s \\ d\widehat{Y}_s &= \left(\frac{1}{2} \|\widehat{Z}_s\|^2 + F_s \right) ds + \widehat{Z}_s^\top dW_s \end{aligned}$$

where

$$f_s := f(\bar{X}_s, \exp(Y_s + \widehat{Y}_s)), \quad F_s := F(\bar{X}_s, \exp(Y_s + \widehat{Y}_s)).$$

We conclude the proof. \square

A.3.4 Proof of Proposition 3

Proof. We will only prove the TD objective (14a) for the time coordinate t , as all derivations can be adopted similarly to its reversed coordinate $s := T - t$.

Given a realization of the parametrized SDE (11a) w.r.t. some fixed step size δt , i.e.,

$$X_{t+\delta t}^\theta = X_t^\theta + (f_t + \sigma Z_\theta(X_t^\theta, t)) \delta t + \delta W_t, \quad \delta W_t \sim \mathcal{N}(\mathbf{0}, \delta t \mathbf{I}),$$

we can represent the trajectory compactly by a sequence of tuples $\mathbf{X}_t^\theta \equiv (X_t^\theta, Z_t^\theta, \delta W_t)$ sampled on some discrete time grids, $t \in \{0, \delta t, \dots, T - \delta t, T\}$. The incremental change of \hat{Y}_t , i.e., the r.h.s. of (11c), can then be computed by

$$\delta \hat{Y}_t(\mathbf{X}_t^\theta) := \left(\frac{1}{2} \|\widehat{Z}(X_t^\theta, t)\|^2 + \nabla \cdot (\sigma \widehat{Z}(X_t^\theta, t) - f_t) + \widehat{Z}(X_t^\theta, t)^\top Z_t^\theta - F_t \right) \delta t + \widehat{Z}(X_t^\theta, t)^\top \delta W_t,$$

where $\widehat{Z}(\cdot, \cdot)$ is the (parametrized) backward policy and we denote $Z_t^\theta := Z_\theta(X_t^\theta, t)$ for simplicity. At the equilibrium when the FBSDE system (11) is satisfied, the SDE (11c) must hold. This suggests the following equality:

$$\widehat{Y}(X_{t+\delta t}^\theta, t + \delta t) = \widehat{Y}(X_t^\theta, t) + \delta \widehat{Y}_t(\mathbf{X}_t^\theta). \quad (37)$$

Hence, we can interpret the r.h.s. of (37) as the single-step TD target $\widehat{\text{TD}}_{t+\delta t}^{\text{single}}$, which yields the expression in (14a). The multi-step TD target can be constructed accordingly as standard practices [51, 52], and either TD target can be used to construct the TD objective for the parametrized function $\hat{Y}_\phi \approx \hat{Y}$, which further yields (16). \square

A.3.5 Proof of Proposition 4

Proof. We first prove the necessity. Suppose the parametrized functions $(Y_\theta, Z_\theta, \hat{Y}_\phi, \widehat{Z}_\phi)$ satisfy the SDEs in (11,12), it can be readily seen that the TD objectives $\mathcal{L}_{\text{TD}}(\phi)$ and $\mathcal{L}_{\text{TD}}(\theta)$ shall both be minimized, as the parametrized functions satisfy (11c,12b). Next, notice that (11) implies

$$\begin{aligned} Y_T^\theta + \widehat{Y}_T^\phi &= \left(Y_0^\theta + \int_0^T dY_t^\theta \right) + \left(\widehat{Y}_0^\phi + \int_0^T d\widehat{Y}_t^\phi \right) \\ \Rightarrow 0 &= \mathbb{E}_{q^\theta} \left[\left(Y_0^\theta + \widehat{Y}_0^\phi \right) + \int_0^T \left(dY_t^\theta + d\widehat{Y}_t^\phi \right) - \left(Y_T^\theta + \widehat{Y}_T^\phi \right) \right] \\ &\stackrel{(*)}{=} \mathbb{E}_{q_0^\theta} [\log \rho_0] + \int_0^T \mathbb{E}_{q_t^\theta} \left[\frac{1}{2} \|Z_t^\theta + \widehat{Z}_t^\phi\|^2 + \nabla \cdot (\sigma \widehat{Z}_t^\phi - f_t) \right] dt - \mathbb{E}_{q_T^\theta} [\log \rho_{\text{target}}] \\ &\stackrel{(**)}{=} \mathbb{E}_{q_0^\theta} [\log \rho_0] + D_{\text{KL}}(q^\theta \| q^\phi) - \mathbb{E}_{q^\theta} \left[\log \frac{\rho_0}{\rho_{\text{target}}} \right] - \mathbb{E}_{q_T^\theta} [\log \rho_{\text{target}}] \\ &= D_{\text{KL}}(q^\theta \| q^\phi), \end{aligned}$$

where (*) is due to (11b,11c) and (**) invokes Proposition 9. The fact that $\mathcal{L}_{\text{IPF}}(\phi) \propto D_{\text{KL}}(q^\theta \| q^\phi) = 0$ (recall Lemma 1) suggests that the objective $\mathcal{L}_{\text{IPF}}(\phi)$ is minimized when (11) holds. Finally, as similar arguments can be adopted to $\mathcal{L}_{\text{IPF}}(\theta) \propto D_{\text{KL}}(q^\phi \| q^\theta) = 0$ when (12) holds, we conclude that all losses are minimized when the parameterized functions satisfy the FBSDE systems (11,12).

We proceed to proving the sufficiency, which is more involved. First, notice that

$$\mathcal{L}_{\text{IPF}}(\phi) \text{ is minimized} \Leftrightarrow D_{\text{KL}}(q^\theta \| q^\phi) = 0 \Leftrightarrow \forall s \in [0, T], Z_s^\theta + \widehat{Z}_s^\phi - \sigma \nabla \log q_s^\theta = 0, \quad (38)$$

$$\mathcal{L}_{\text{IPF}}(\theta) \text{ is minimized} \Leftrightarrow D_{\text{KL}}(q^\phi \| q^\theta) = 0 \Leftrightarrow \forall t \in [0, T], Z_t^\theta + \widehat{Z}_t^\phi - \sigma \nabla \log q_t^\phi = 0, \quad (39)$$

as implied by (27). If $\mathcal{L}_{\text{TD}}(\phi)$ and $\mathcal{L}_{\text{TD}}(\theta)$ are minimized, the following relations must also hold

$$d\widehat{Y}_t^\phi = \left(\frac{1}{2} \|\widehat{Z}_t^\phi\|^2 + \nabla \cdot (\sigma \widehat{Z}_t^\phi - f_t) + Z_t^{\theta \top} \widehat{Z}_t^\phi - F_t \right) dt + \widehat{Z}_t^{\phi \top} dW_t, \quad (40)$$

$$dY_s^\theta = \left(\frac{1}{2} \|Z_s^\theta\|^2 + \nabla \cdot (\sigma Z_s^\theta + f_s) + Z_s^{\theta \top} \widehat{Z}_s^\phi - F_s \right) dt + Z_s^{\theta \top} dW_s. \quad (41)$$

Now, notice that the Fokker Plank equation of the parametrized forward SDE (25a) obeys

$$\frac{\partial q_t^\theta}{\partial t} = -\nabla \cdot (q_t^\theta (f_t + \sigma Z_t^\theta)) + \frac{1}{2} \sigma^2 \Delta q_t^\theta,$$

which implies that (c.f. Lemma 7),

$$\frac{\partial \log q_t^\theta}{\partial t} = -\nabla \cdot (f_t + \sigma Z_t^\theta) - \nabla \log q_t^{\theta \top} (f_t + \sigma Z_t^\theta) + \frac{\sigma^2}{2} (\Delta \log q_t^\theta + \|\nabla \log q_t^\theta\|^2). \quad (42)$$

Invoking Ito lemma yields:

$$\begin{aligned} d \log q_t^\theta &= \frac{\partial \log q_t^\theta}{\partial t} dt + \left[\nabla \log q_t^{\theta \top} (f_t + \sigma Z_t^\theta) + \frac{\sigma^2}{2} \Delta \log q_t^\theta \right] dt + \sigma \nabla \log q_t^{\theta \top} dW_t \\ &\stackrel{(42)}{=} \left[-\nabla \cdot (f_t + \sigma Z_t^\theta) + \sigma^2 \Delta \log q_t^\theta + \frac{\sigma^2}{2} \|\nabla \log q_t^\theta\|^2 \right] dt + \sigma \nabla \log q_t^{\theta \top} dW_t \\ &= \left[-\nabla \cdot (f_t + \sigma Z_t^\theta - \sigma^2 \nabla \log q_t^\theta) + \frac{1}{2} \|\sigma \nabla \log q_t^\theta\|^2 \right] dt + \sigma \nabla \log q_t^{\theta \top} dW_t \\ &\stackrel{(*)}{=} \left[-\nabla \cdot (f_t + \sigma Z_t^\theta - \sigma (Z_t^\theta + \widehat{Z}_t^\phi)) + \frac{1}{2} \|Z_t^\theta + \widehat{Z}_t^\phi\|^2 \right] dt + (Z_t^\theta + \widehat{Z}_t^\phi)^\top dW_t \\ &= \left[\nabla \cdot (\sigma \widehat{Z}_t^\phi - f_t) + \frac{1}{2} \|Z_t^\theta + \widehat{Z}_t^\phi\|^2 \right] dt + (Z_t^\theta + \widehat{Z}_t^\phi)^\top dW_t, \end{aligned} \quad (43)$$

where (*) is due to (38). Subtracting (40) from (43) yields

$$d \log q_t^\theta - d \widehat{Y}_t^\phi = \left(\frac{1}{2} \|Z_t^\theta\|^2 + F_t \right) dt + Z_t^{\theta \top} dW_t. \quad (44)$$

Now, using the fact that $Z_\theta := \sigma \nabla Y_\theta$ and $\widehat{Z}_\phi := \sigma \nabla \widehat{Y}_\phi$, we know that

$$Z_t^\theta + \widehat{Z}_t^\phi - \sigma \nabla \log q_t^\theta = 0 \Rightarrow Y_t^\theta + \widehat{Y}_t^\phi = \log q_t^\theta + c_t,$$

for some function $c_t \equiv c(t)$. Hence, (44) becomes

$$dY_t^\theta - dc_t = \left(\frac{1}{2} \|Z_t^\theta\|^2 + F_t \right) dt + Z_t^{\theta \top} dW_t. \quad (45)$$

Now we prove that $\forall t \in (0, T), dc_t = 0$ by contradiction. First, notice that c_t can be derived analytically as

$$\begin{aligned} c_t &= Y_t^\theta + \widehat{Y}_t^\phi - \log q_t^\theta \\ &= \int_0^t (dY_\tau^\theta + d\widehat{Y}_\tau^\phi - d \log q_\tau^\theta) \\ &\stackrel{(*)}{=} \int_0^t \left(\left(\frac{\partial Y_\tau^\theta}{\partial \tau} + \nabla Y_\tau^{\theta \top} (f_\tau + \sigma Z_\tau^\theta) + \frac{\sigma^2}{2} \Delta Y_\tau^\theta \right) - \left(\frac{1}{2} \|Z_\tau^\theta\|^2 + F_\tau \right) \right) d\tau \\ &\quad + \int_0^t (\sigma \nabla Y_\tau^{\theta \top} dW_\tau - Z_\tau^{\theta \top} dW_\tau) \\ &\stackrel{(**)}{=} \int_0^t \left(\frac{\partial Y_\tau^\theta}{\partial t} - \left(-\nabla Y_\tau^{\theta \top} f_\tau - \frac{1}{2} \|\sigma \nabla Y_\tau^\theta\|^2 - \frac{\sigma^2}{2} \Delta Y_\tau^\theta + F_\tau \right) \right) d\tau, \end{aligned} \quad (46)$$

where (*) invokes the following Ito lemma and substitutes (44),

$$dY_\tau^\theta = \frac{\partial Y_\tau^\theta}{\partial \tau} d\tau + \left[\nabla Y_\tau^{\theta \top} (f_\tau + \sigma Z_\tau^\theta) + \frac{\sigma^2}{2} \Delta Y_\tau^\theta \right] dt + \sigma \nabla Y_\tau^{\theta \top} dW_\tau,$$

and (**) substitutes the definition $Z_\tau^\theta := \sigma \nabla Y_\tau^\theta$. Equation (46) has an intriguing implication, as one can verify that its integrand is the residual of the parametrized HJB $Y_\theta = -u_\theta \approx -u$ (recall (7) and (8)). It is straightforward to see that, the residual shall also be preserved after the parametrized HJB is

expanded by Ito lemma w.r.t. the backward parametrized SDE (25b). That is, the following equation similar to (45) must hold for the function $c_s := c(T - t)$:

$$dY_s^\theta + dc_s = \left(\frac{1}{2} \|Z_s^\theta\|^2 + \nabla \cdot (f_s + \sigma Z_s^\theta) + Z_s^{\theta\top} \widehat{Z}_s^\phi - F_s \right) dt + Z_s^{\theta\top} dW_s,$$

which contradicts (41). Hence, we must have $dc_s = dc_t = 0$, and (45) becomes

$$dY_t^\theta = \left(\frac{1}{2} \|Z_t^\theta\|^2 + F_t \right) dt + Z_t^{\theta\top} dW_t. \quad (47)$$

In short, we have shown that, for the parametrized forward (25a) and backward (25b) SDEs, the fact that (40, 41) hold implies that (47) holds, providing \mathcal{L}_{IPF} is minimized. The exact same statement can be repeated to prove that

$$d\widehat{Y}_s^\phi = \left(\frac{1}{2} \|\widehat{Z}_s^\phi\|^2 + F_s \right) ds + \widehat{Z}_s^{\phi\top} dW_s. \quad (48)$$

Therefore, if the combined objectives are minimized, *i.e.*, (38, 39, 40, 41) hold, the parametrized functions $(Y_\theta, Z_\theta, \widehat{Y}_\phi, \widehat{Z}_\phi)$ satisfy (25, 40, 47, 41, 48), *i.e.*, they satisfy the FBSDE systems (11, 12) in Theorem 2. \square

A.4 Additional Derivations & Remarks in Sec. 3 and 4

A.4.1 Hopf-Cole transform

Recall the Hopf-Cole transform

$$\Psi(x, t) := \exp(-u(x, t)), \quad \widehat{\Psi}(x, t) := \rho(x, t) \exp(u(x, t)).$$

Standard ordinary calculus yields

$$\nabla \Psi = -\exp(-u) \nabla u, \quad \Delta \Psi = \exp(-u) [\|\nabla u\|^2 - \Delta u], \quad (49)$$

$$\nabla \widehat{\Psi} = \exp(u) (\rho \nabla u + \nabla \rho), \quad \Delta \widehat{\Psi} = \exp(u) [\rho \|\nabla u\|^2 + 2\nabla \rho^\top \nabla u + \Delta \rho + \rho \Delta u]. \quad (50)$$

Hence, we have

$$\begin{aligned} \frac{\partial \Psi}{\partial t} &= \exp(-u) \left(-\frac{\partial u}{\partial t} \right) \\ &\stackrel{(7)}{=} \exp(-u) \left(-\frac{1}{2} \|\sigma \nabla u\|^2 + \nabla u^\top f + \frac{1}{2} \sigma^2 \Delta u + F \right) \\ &\stackrel{(49)}{=} -\frac{1}{2} \sigma^2 \Delta \Psi - \nabla \Psi^\top f + F \Psi, \end{aligned} \quad (51)$$

$$\begin{aligned} \frac{\partial \widehat{\Psi}}{\partial t} &= \exp(u) \left(\frac{\partial \rho}{\partial t} + \rho \frac{\partial u}{\partial t} \right) \\ &\stackrel{(7)}{=} \exp(u) \left(\left(\nabla \cdot (\rho (\sigma^2 \nabla u - f)) + \frac{1}{2} \sigma^2 \Delta \rho \right) + \rho \left(\frac{1}{2} \|\sigma \nabla u\|^2 - \nabla u^\top f - \frac{1}{2} \sigma^2 \Delta u - F \right) \right) \\ &= \exp(u) \left(\sigma^2 \left(\rho \Delta u + \nabla \rho^\top \nabla u + \frac{1}{2} \Delta \rho + \frac{\rho}{2} \|\nabla u\|^2 - \frac{\rho}{2} \Delta u \right) - \nabla \rho^\top f - \rho \nabla \cdot f - \rho \nabla u^\top f - \rho F \right) \\ &\stackrel{(50)}{=} \frac{1}{2} \sigma^2 \Delta \widehat{\Psi} - \nabla \widehat{\Psi}^\top f - \widehat{\Psi} \nabla \cdot f - \widehat{\Psi} F, \end{aligned} \quad (52)$$

which yields (9) by noticing that $\nabla \cdot (\widehat{\Psi} f) = \nabla \widehat{\Psi}^\top f + \widehat{\Psi} \nabla \cdot f$.

A.4.2 Remarks on convergence

The alternating optimization scheme proposed in Alg. (1) can be compactly presented as $\min_\phi D_{\text{KL}}(q^\theta \| q^\phi) + \mathbb{E}_{q^\phi}[\mathcal{L}_{\text{TD}}(\phi)]$ and $\min_\theta D_{\text{KL}}(q^\phi \| q^\theta) + \mathbb{E}_{q^\phi}[\mathcal{L}_{\text{TD}}(\theta)]$. Despite that the procedure seems to resemble IPF, which optimizes between $\min_\phi D_{\text{KL}}(q^\phi \| q^\theta)$ and $\min_\theta D_{\text{KL}}(q^\theta \| q^\phi)$, we stress that they differ from each other in that the the KLs are constructed with different directions.

In cases where the TD objectives are discarded, prior work [24] has proven that minimizing the forward KLs admit similar convergence to standard IPF (which minimizes the reversed KLs). This is essentially the key to developing scalable methods, since the parameter being optimized (*e.g.*, θ in $D_{\text{KL}}(q^\phi|q^\theta)$) in forward KLs differs from the parameter used to sample expectation (*e.g.*, \mathbb{E}_{q^ϕ}). Therefore, the computational graph of the SDEs can be dropped, yielding a computationally much efficient framework. These advantages have been adopted in [24, 27] and also this work for solving higher-dimensional problems.

However, when we need TD objectives to enforce the MF structure, as appeared in all the MFGs in this work, the combined objective does not correspond to IPF straightforwardly. Despite that the alternating procedure in Alg. (1) is mainly inspired by prior SB methods [24, 27], the training process of DeepGSB is perhaps closer to TRPO [55], which iteratively updates the policy using the off-policy samples generated from the previous stage: $\pi^{(i+1)} = \arg \min_{\pi} D_{\text{KL}}(\pi^{(i)}||\pi) + \mathbb{E}_{\pi^{(i)}}[\mathcal{L}(\pi)]$. TRPO is proven to enjoy monotonic improvement over iterations (*i.e.*, local convergence).

A.4.3 Functional derivative of MF potential functions

Given a functional $\mathcal{F} : \mathcal{P}(\mathbb{R}^d) \rightarrow \mathbb{R}$ on the space of probability measures, its functional derivative $F(x, \rho) := \frac{\delta \mathcal{F}(\rho)}{\delta \rho}(x)$ satisfies the following equation

$$\lim_{h \rightarrow 0} \frac{\mathcal{F}(\rho + hw) - \mathcal{F}(\rho)}{h} = \int_{\mathbb{R}^d} F(x, \rho) w(x) dx$$

for any function $w \in L^2(\mathbb{R}^d)$. Hence, the derivative of the entropy MF functional $\mathcal{F}_{\text{entropy}} := \int_{\mathbb{R}^d} \rho(x) \log \rho(x) dx$ can be derived as

$$\begin{aligned} & \lim_{h \rightarrow 0} \frac{1}{h} \left(\mathcal{F}_{\text{entropy}}(\rho + hw) - \mathcal{F}_{\text{entropy}}(\rho) \right) \\ &= \lim_{h \rightarrow 0} \frac{1}{h} \left(\int_{\mathbb{R}^d} \left(hw(x) \log \rho(x) + \rho(x) \frac{hw(x)}{\rho(x)} + \mathcal{O}(h^2) \right) dx \right) \\ &= \int_{\mathbb{R}^d} \left(w(x) \log \rho(x) + w(x) \right) dx = \int_{\mathbb{R}^d} \underbrace{(\log \rho(x) + 1)}_{:= F_{\text{entropy}}(x, \rho)} w(x) dx. \end{aligned} \quad (53)$$

Similarly, consider the congestion MF functional $\mathcal{F}_{\text{congestion}} := \int_{\mathbb{R}^d} \int_{\mathbb{R}^d} \frac{1}{\|x-y\|^2+1} \rho(x) \rho(y) dx dy$. Its derivation can be computed by

$$\begin{aligned} & \lim_{h \rightarrow 0} \frac{1}{h} \left(\mathcal{F}_{\text{congestion}}(\rho + hw) - \mathcal{F}_{\text{congestion}}(\rho) \right) \\ &= \lim_{h \rightarrow 0} \frac{1}{h} \left(\int_{\mathbb{R}^d} \int_{\mathbb{R}^d} \frac{1}{\|x-y\|^2+1} \left(\rho(x) hw(y) + hw(x) \rho(y) + \mathcal{O}(h^2) \right) dx dy \right) \\ &= \int_{\mathbb{R}^d} \int_{\mathbb{R}^d} \frac{1}{\|x-y\|^2+1} \left(\rho(x) w(y) + w(x) \rho(y) \right) dx dy \\ &= \int_{\mathbb{R}^d} \int_{\mathbb{R}^d} \frac{2}{\|x-y\|^2+1} dy w(x) dx. \end{aligned} \quad (54)$$

$:= F_{\text{congestion}}(x, \rho)$

We hence conclude the expressions of F_{entropy} and $F_{\text{congestion}}$ in (17).

A.5 Experiment Details

A.5.1 Setup

Hyperparameters Table 6 summarizes the hyperparameters in each MFG, including the dimension d of the state space, the diffusion scalar σ , the time horizon T , the discretized time step δt (and δs), the MF base drift $f(x, \rho)$, the MF interaction $F(x, \rho)$, and the mean/covariance of the boundary distributions ρ_0 and ρ_{target} (note that all MFGs adopt Gaussians as their boundary distributions). Note that in the 1000-dimensional opinion MFG, we multiply the polarized dynamic $\bar{f}_{\text{polarize}}$ by 6 to

Table 6: Hyperparameters in each MFG. Note that $\mathbf{0} \in \mathbb{R}^d$ denotes zero vector, $\mathbf{I} \in \mathbb{R}^{d \times d}$ denotes identity matrix, and $\text{diag}(\mathbf{v}) \in \mathbb{R}^{d \times d}$, where $\mathbf{v} \in \mathbb{R}^d$, denotes diagonal matrix.

	GMM	V-neck	S-tunnel	Opinion	
d	2	2	2	2	1000
σ	1	1	1	0.1	0.5
T	1	2	3	3	3
δt	0.01	0.01	0.01	0.01	0.006
$f(x, \rho)$	$[0, 0]^\top$	$[6, 0]^\top$	$[6, 0]^\top$	$\bar{f}_{\text{polarize}}$	$6 \cdot \bar{f}_{\text{polarize}}$
Diffusion steps	100	200	300	300	500
K^7	250	250	500	100	250
Alternating stages ⁸	40	40	30	40	90
Total training steps	20k	20k	30k	8k	45k
Mean of ρ_0	$\mathbf{0}$	$\begin{bmatrix} -7 \\ 0 \end{bmatrix}$	$\begin{bmatrix} -11 \\ -1 \end{bmatrix}$	$\mathbf{0}$	$\mathbf{0}$
Mean of ρ_{target}	$e^{16 \cdot (\frac{\pi}{4})i}$, $i \in \{0, \dots, 7\}$	$\begin{bmatrix} 7 \\ 0 \end{bmatrix}$	$\begin{bmatrix} 11 \\ 1 \end{bmatrix}$	$\mathbf{0}$	$\mathbf{0}$
Covariance of ρ_0	\mathbf{I}	$0.2\mathbf{I}$	$0.5\mathbf{I}$	$\text{diag}\left(\begin{bmatrix} 0.5 \\ 0.25 \end{bmatrix}\right)$	$\text{diag}\left(\begin{bmatrix} 4 \\ 0.25 \\ \vdots \\ 0.25 \end{bmatrix}\right)$
Covariance of ρ_{target}	\mathbf{I}	$0.2\mathbf{I}$	$0.5\mathbf{I}$	$3\mathbf{I}$	$3\mathbf{I}$

ensure that the high-dimensional dynamics yield polarization within the time horizon. Meanwhile, a smaller step size $\delta t = 0.006$ is adopted so that the discretization error from the relatively large drift is mitigated. As mentioned in Sec. 4, we adopt zero and constant base drift f respectively for GMM and V-neck/S-tunnel.

Training All experiments are conducted on 3 TITAN RTXs and 1 TITAN V100, where the V100 is located on the Amazon Web Service (AWS). We use the multi-step TD targets in (15) for all experiments and adopt huber norm for the TD loss in (16). As for the FK consistency loss \mathcal{L}_{FK} , we use ℓ_1 norm for GMM and opinion MFGs, and huber norm for the rest.

Network architecture All networks $(Y_\theta, Z_\theta, \hat{Y}_\phi, \hat{Z}_\phi)$ take (x, t) as inputs and follow

$$\text{out} = \text{out_mod}(\text{x_mod}(x) + \text{t_mod}(\text{timestep_embedding}(t))),$$

where $\text{timestep_embedding}(\cdot)$ is the standard sinusoidal embedding.

For crowd navigation MFGs, these modules consist of 2 to 4 fully-connected layers (Linear) followed by the Sigmoid Linear Unit (SiLU) activation functions [70], *i.e.*,

$$\begin{aligned} \text{t_mod} &= \text{Linear} \rightarrow \text{SiLU} \rightarrow \text{Linear} \\ \text{x_mod} &= \text{Linear} \rightarrow \text{SiLU} \rightarrow \text{Linear} \rightarrow \text{SiLU} \rightarrow \text{Linear} \rightarrow \text{SiLU} \rightarrow \text{Linear} \\ \text{out_mod} &= \text{Linear} \rightarrow \text{SiLU} \rightarrow \text{Linear} \rightarrow \text{SiLU} \rightarrow \text{Linear} \end{aligned}$$

As for 1000-dimensional opinion MFG, we keep the same t_mod and out_mod but adopt residual networks with 5 residual blocks for x_mod . For DeepGSB-ac, we set the hidden dimension of Linear to 256 and 128 respectively for the policy networks (Z_θ, \hat{Z}_ϕ) and the critic networks (Y_θ, \hat{Y}_ϕ) , whereas for DeepGSB-c, we set the hidden dimension of Linear to 200 for the critic networks (Y_θ, \hat{Y}_ϕ) .

⁷We note that, unlike SB-FBSDE [27], the number of training iterations at each stage (*i.e.*, the K in Alg. 1) is kept *fixed* throughout training.

⁸Here, we refer *one alternating stage* to a complete cycling through $2K$ training iterations in Alg. 1.

Implementation of prior methods [14–16] All of our experiments are implemented with PyTorch [71]. Hence, we re-implement the method in Ruthotto et al. [14] by migrating their Julia codebase⁹ to PyTorch. As for Lin et al. [15], their official PyTorch implementation is publicly available.¹⁰ Finally, we implement Chen [16] by ourselves. Since prior methods [14–16] were developed for a smaller class of MFGs compared to our DeepGSB (recall Table 1), we need to relax the setup of the MFG in order for them to yield reasonable results in Fig. 5 and 8. Specifically, we soften the obstacle costs, so that [14, 15] can differentiate them properly, and keep the same KL penalty at $u(x, T) \approx D_{\text{KL}}(\rho(x, T) || \rho_{\text{target}}(x))$ as adopted in [14, 15]. We stress that neither of the methods [14, 15] works well with the discontinuous F_{obstacle} in (17). Finally, we discretize the 2-dimensional state space of GMM into a 40×40 grid with 50 time steps for [16]. We note that the complexity of [16] scales as $\mathcal{O}(\tilde{T}D^2)$, where \tilde{T} and D are respectively the number of time and spatial grids, *i.e.*, $\tilde{T} = 50$ and $D = 1600$.

Evaluation We approximate the Wasserstein distance with the Sinkhorn divergence using the geomLoss package.¹¹ The Sinkhorn divergence interpolates between Wasserstein (blur = 0) and kernel (blur = ∞) distance given the hyperparameter blur. We set blur = 0.05 in Table 3.

A.5.2 Additional experiments

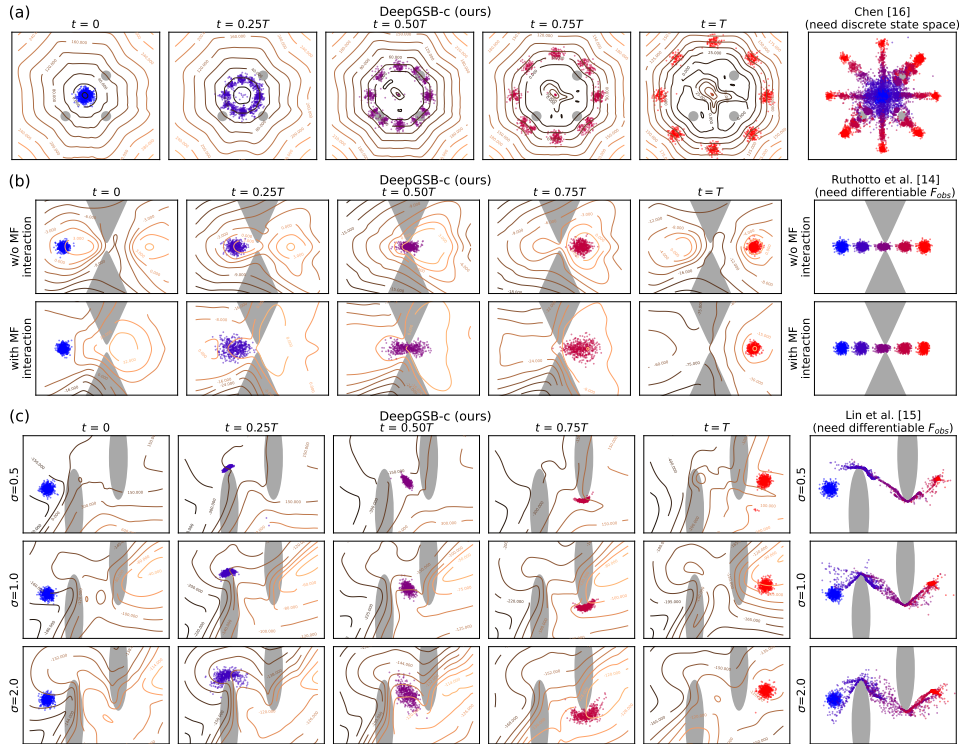


Figure 8: Same setup as in Fig. 5 except for **DeepGSB-c**. This figure is best viewed in color.

Figures 8 and 9 reports the results for **DeepGSB-c**. On crowd navigation MFGs, the population snapshots guided by DeepGSB-c are visually indistinguishable from DeepGSB-ac (see Fig. 8 vs. 5) despite the visual difference in their contours. As for 1000-dimensional opinion MFG, both DeepGSB-c and DeepGSB-ac are able to guild the population opinions toward desired ρ_{target} without the entropy interaction F_{entropy} . Figure 9 reports the results of DeepGSB-c in such cases. We note, however, that when F_{entropy} is enabled, DeepGSB-ac typically performs better than DeepGSB-c in terms of convergence to ρ_{target} and training stability.

⁹<https://github.com/EmoryMLIP/MFGnet.jl>. The repository is licensed under MIT License.

¹⁰<https://github.com/atlin23/apac-net>. The repository does not specify licenses.

¹¹<https://github.com/jeanfeydy/geomLoss>. The repository is licensed under MIT License.

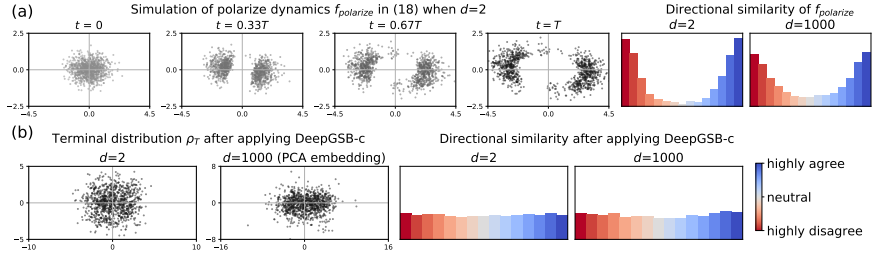


Figure 9: (a) Visualization of polarized dynamics $\bar{f}_{\text{polarize}}$ in 2- and 1000-dimensional opinion space, where the *directional similarity* [3] counts the histogram of cosine angle between pairwise opinions at the terminal distribution ρ_T . (b) **DeepGSB-c** guides ρ_T to approach moderated distributions, hence *depolarizes* the opinion dynamics. Note that we adopt $F := 0$ for DeepGSB-c. We use the first two principal components to visualize $d=1000$.